

Cooperative Diversity for Fading Channels in the Presence of Impulsive Noise

by

Suhail Ibrahim Al-Dharrab

A thesis
presented to the University of Waterloo
in fulfillment of the
thesis requirement for the degree of
Master of Applied Science
in
Electrical and Computer Engineering

Waterloo, Ontario, Canada, 2008

© Suhail Ibrahim Al-Dharrab 2008

AUTHOR'S DECLARATION

I hereby declare that I am the sole author of this thesis. This is a true copy of the thesis, including any required final revisions, as accepted by my examiners.

I understand that my thesis may be made electronically available to the public.

Abstract

Although there already exists a rich literature on cooperative diversity, current results are mainly restricted to the conventional assumption of additive white Gaussian noise (AWGN). AWGN model realistically represents the thermal noise at the receiver, but ignores the impulsive nature of atmospheric noise, electromagnetic interference, or man-made noise which might be dominant in many practical applications. In this thesis, we investigate the performance of cooperative communication over Rayleigh fading channels in the presence of impulsive noise modeled by Middleton Class A noise.

We consider a multi-relay network with amplify-and-forward relaying and orthogonal cooperation protocol. As for the coding across the relays, we employ either space-time coding or repetition coding. For each scheme, we assume various scenarios based on relays' location and quantify the diversity advantages through the derivation of the pairwise error probability. Based on the minimization of a union bound on the error rate performance, we further propose optimal power allocation schemes and demonstrate significant performance gains over their counterparts with equal power allocation. We finally present an extensive Monte Carlo simulation to confirm our analytical results and corroborate on our results.

Acknowledgements

Praises and thankfulness are for Allah, the most merciful and most compassionate for bestowing me with his great bounties and granting me the strength to seek knowledge.

My deepest appreciation and profuse thanks go to my adviser, Prof. Murat Uysal, who has provided me with an endless support, assistance, and motivation throughout the MASc. program. His insightful suggestions, invaluable advices, kindness, and patience have influenced me in many aspects. I also would like to thank my thesis committee members Prof. Amir Khandani and Prof. Liang-Liang Xie for their valuable time devoted in reviewing my thesis.

My thanks extend to King Fahd University of Petroleum and Minerals for their financial support in completing my MASc. program. I thank the Ministry of Higher Education and Saudi Cultural Bureau in Canada for their support.

My heartiest thanks go to my parents and siblings for their love, kindness, and patience. I will be forever indebted to them for their unconditional trust and willingness to endure with me the challenges of my endeavors.

I would like to thank my colleagues Osama Amin, Muhammed Hakeem, and Jawwad Hussain for their insightful discussions and cooperation at the beginning of my program.

Last, but not least, I express my deep appreciation to numerous people who have contributed to my education and my well-being at University of Waterloo and elsewhere, even with a genuine smile in my face.

Dedication

To my parents

Table of Contents

List of Figures	viii
List of Tables	ix
List of Abbreviations	x
Chapter 1 Introduction.....	1
1.1 Impulsive Noise	1
1.2 Overview of Diversity Techniques and Cooperative Diversity	3
1.2.1 Transmit Diversity	5
1.2.2 Cooperative Diversity	6
1.3 Research Motivation	7
1.4 Thesis Outline	8
Chapter 2 System Model	9
2.1 Fading Channel Model.....	9
2.2 Impulsive Noise Model.....	10
2.3 Transmission Model.....	12
2.3.1 Space-Time Coded Cooperative Diversity (STC-CD) Scheme	12
2.3.2 Repetition-based Cooperative Diversity (RB-CD) Scheme.....	14
2.4 Receiver	14
Chapter 3 Error Rate Performance Analysis	16
3.1 Performance of STC-CD Scheme	16
3.1.1 PEP for Spatially Dependent Noise	16
3.1.2 PEP for Spatially Independent Noise.....	19
3.2 Performance of RB-CD Scheme	20
3.2.1 PEP for Spatially Dependent Noise	20
3.2.2 PEP for Spatially Independent Noise.....	22
3.3 Diversity Gain Analysis.....	23
3.4 Union Bound on BER Performance.....	24
Chapter 4 Optimum Power Allocation	26
4.1 Optimization of Power Allocation for Multi-Relay System	26
4.2 Numerical Results	26
4.2.1 Highly Impulsive (HI) Noise	27

4.2.2 Near Gaussian (NG) Noise	29
Chapter 5 Simulation Results and Discussion	31
5.1 BER Performance for OPA in Multi-Relay Channel	31
Chapter 6 Conclusions	40
Appendix	41
Bibliography	42

List of Figures

Figure 2.1: Relay-assisted transmission.....	9
Figure 2.2: Probability density function of Middleton Class A model.....	11
Figure 3.1: Comparison of derived PEP expression and Chernoff bound of STC-CD scheme in spatially dependent noise.	18
Figure 3.2: Comparison of derived PEP expression and Chernoff bound of STC-CD scheme in spatially independent noise.	20
Figure 3.3: Comparison of derived PEP expression and Chernoff bound of RB-CD scheme in spatially dependent noise.	21
Figure 3.4: Comparison of derived PEP expression and Chernoff bound of RB-CD scheme in spatially independent noise.	23
Figure 5.1: Performance of Alamouti-coded scheme in HI, MI and NG noise for scenario 1.....	32
Figure 5.2: BER performance of Alamouti-coded scheme for various relays' locations	33
Figure 5.3: BER performance of repetition-based scheme for various relays' locations	34
Figure 5.4: Derived PEP for Alamouti-coded cooperative scheme for different relays' locations	35
Figure 5.5: Derived PEP for repetition-based cooperative scheme for different relays' locations	35
Figure 5.6: Performance comparison of OPA and EPA in HI noise for STC-CD scheme	36
Figure 5.7: Performance comparison of OPA and EPA in near Gaussian channel.....	37
Figure 5.8: Performance comparison of OPA and EPA in HI noise for RB-CD scheme.....	38
Figure 5.9: Performance comparison between spatially dependent and independent impulsive noise	39

List of Tables

Table 4-1: Optimum power allocation values for STC-CD in HI noise.....	28
Table 4-2: Optimum power allocation values for RB-CD in HI noise.....	28
Table 4-3: Optimum power allocation values for near Gaussian channel for STC-CD.....	29
Table 4-4: Optimum power allocation values for near Gaussian channel for RB-CD.....	30

List of Abbreviations

WLAN	Wireless Local Area Network
WSN	Wireless Sensor Network
MIMO	Multiple-Input Multiple-Output
AWGN	Additive White Gaussian Noise
EMI	Electromagnetic Interference
UMTS	Universal Mobile Telecommunications System
HI	Highly Impulsive
MI	Moderate Impulsive
NG	Near Gaussian
EPA	Equal Power Allocation
OPA	Optimum Power Allocation
MRC	Maximal Ratio Combining
CSI	Channel State Information
STC	Space-Time Coding
STBC	Space-Time Block Code
STTC	Space-Time Trellis Code
AF	Amplify-and-Forward
DF	Decode-and-Forward
TDMA	Time Division Multiple Access
STC-CD	Space-Time Coded Cooperative Diversity
RB-CD	Repetition-Based Cooperative Diversity
MDR	Minimum Distance Receiver
PEP	Pairwise Error Probability
BER	Bit Error Rate
SNR	Signal-to-Noise Ratio

Chapter 1

Introduction

Today's communication networks support various applications such as broadband data and Internet access, multimedia broadcasting, video conferencing, and video-on-demand among others. The idea of reliable and ubiquitous information access has led to the deployment of a variety of wireless communication systems [1]. Cellular networks, wireless local area network (WLANs), wireless ad hoc networks, wireless sensor networks (WSNs), and vehicular ad hoc networks (VANETs) are some examples of rapidly growing subfields in wireless communication. Due to the increasing demand on communication systems, there have been intensive research efforts to enhance data rate and reliability of these systems.

A powerful technique proposed in late 1990's to improve the performance in wireless systems is multiple-input multiple-output (MIMO) communication which involves the deployment of multiple transmit and/or receive antennas [2]. In some applications, implementation of multiple antennas for end-users or handsets is difficult due to the size, cost, and hardware limitations [3]. An alternative method is to have single-antenna users share their resources and form a virtual MIMO system exploiting each other's antennas. This technique is called cooperative diversity or cooperative communication and has received a growing attention in the last five years or so [4, 5].

Although there has been already a rich literature on cooperative communication, the existing works are mainly limited to the assumption of additive white Gaussian noise (AWGN). This assumption reflects the effect of thermal noise at receiver; however, it does not incorporate man-made noise and electromagnetic interference (EMI), which cause impulsive noise that is prevalent in many wireless communication systems [6]. This motivates us to investigate cooperative communication in the presence of impulsive noise. In the forthcoming sections, we provide some background material for impulsive noise and cooperative communication, which will be the basis for the later chapters.

1.1 Impulsive Noise

Impulsive noise is prevalent in many wireless communication applications. For instance, automotive ignition noise, power transmission lines, and arc generating circuit components are examples of impulsive noise sources which are encountered mainly in metropolitan areas [7]. In

indoor wireless communication, devices with electromechanical switches such as electrical motors in elevators, refrigerators units, photocopy machines, and printers are considered as impulsive noise sources. Furthermore, microwave ovens, cash register receipt printers, gas-powered engines, and compressor motors produce impulsive noise on frequency bands which coincide with the operating frequencies of current cellular and wireless local area networks [8], [9].

Measurements of impulsive noise in urban areas have motivated many researchers to characterize impulsive noise by empirical models. In [8], Blackard and Rappaport investigate impulsive noise measurements in office building and retail stores at operating frequencies of 918 MHz, 2.44 GHz, and 4 GHz with a 40 MHz bandwidth. Operating frequencies of 918 MHz and 2.44 GHz are of special interest since they lie in industrial, scientific, and medical (ISM) band. Further in [10], Blankenship and Rappaport characterize impulsive noise at 450 MHz band for urban hospitals and clinics. For universal mobile telecommunications system (UMTS) frequency channels in urban areas, measurements of impulsive noise are analyzed in [11].

There are also several models in literature to statistically model non-Gaussian impulsive noise. In [12], Hall proposes an exogenous model for impulsive model, where impulsive noise is generated as a product of two independent random processes. In exogenous models, a slowly varying random process modulates a narrowband Gaussian process and this modulating process has a probability density function that satisfies the condition of the existence of Fredholm type-I integral equation given in [13]. In [14], impulsive noise has been approximated using spherically invariant random processes (SIRP), which are generalizations of Gaussian processes. In [15], Shao and Nikias propose a symmetric stable distribution, which is characterized by an exponent term α and known as symmetric α -stable ($S\alpha S$) distribution.

Another statistical model for impulsive noise is Middleton's model which is widely adopted in the literature due to analytical tractability, reproducibility, canonical and constructive properties of this model [16, 17]. This model is independent of the waveform and propagation law of the effecting interference emitters [17] and is shown to provide good agreement with empirical measurements in various environments [16]. Three distinct classes for Middleton model are available based on the interference characteristic and bandwidth of noise. Middleton Class A model is valid when the bandwidth of noise is less than that of the receiver front-end and interference waveforms produce

negligible transients at the receiver. If the noise bandwidth exceeds receiver front-end bandwidth and interference waveforms result in significant transients, Class B model becomes valid. Class C, on the other hand, is considered as a mixture of Class A and B models. In this thesis, we consider Middleton Class A to represent impulsive noise in the cooperative communication system under consideration.

1.2 Overview of Diversity Techniques and Cooperative Diversity

Signals propagating through wireless channels are deteriorated by large-scale and small-scale impairments. Large-scale impairments include path loss effect, which quantifies the reduction in average received power as a function of distance from the transmitter. In free space propagation model, the power of received signal is given by

$$P_r = P_t G_t G_r \left(\frac{\lambda}{4\pi d} \right)^2 \quad (1.1)$$

where P_r and P_t are receive and transmit powers, G_r and G_t are receive and transmit antenna gains, λ is the wavelength of the carrier signal, and d is the distance between transmitter and receiver. As observed from (1.1), P_r is inversely proportional to d . In general, we have $P_r \propto d^{-n}$, where n is called the path loss exponent and given in [18] for various environments. Further discussion on path loss models such as Okumura-Hara and Lee's path loss models can be found in [18]. Another large-scale impairment is shadowing, which results from the geometry and existence of obstacles larger than wavelength of transmitted signal, such as trees, hills, and buildings. This causes random fluctuations in strength of received signal. Shadowing is statistically modeled by log-normal distribution.

The major performance-limiting factor in wireless communication systems is multipath-induced fading which is the small-scale impairment. Transmitted signals follow different paths resulting in multipath propagation, and due to reflection from obstacles and scattering objects, delayed versions of transmitted signals are received. Under assumptions of non-line-of-sight and large number of paths, the central limit theorem can be applied and real and imaginary components of multiplicative channel attenuation are modeled as independent Gaussian processes. Therefore, fading amplitude (or envelope) will have Rayleigh distribution, which is given by

$$f_{|h|}(x) = \frac{2x}{\Omega} \exp\left(-\frac{x^2}{\Omega}\right), \quad x \geq 0 \quad (1.2)$$

where $|h|$ is a random variable representing fading amplitude and $\Omega = E[|h|^2] = 2\sigma^2$ is average fading power. For normalized average power, we have $\Omega = 1$ [19].

Multipath fading severely degrades the link performance and powerful countermeasures such as diversity techniques should be employed to maintain an acceptable performance. One diversity technique to mitigate fading is frequency diversity. In frequency diversity, transmitted signal is sent over different frequency slots, where adjacent slots are separated by more than the channel coherence bandwidth. This ensures that independent fading affects different frequency slots. One drawback of frequency diversity technique is the extra bandwidth requirement [18].

Another diversity method is time diversity technique, which is implemented by transmitting the message over different time slots with separation between adjacent time slots larger than coherence time. Time diversity technique requires application of interleaving and proper channel coding such as linear block codes or convolutional codes to ensure that independent fading affect different time slots [20]. This technique sacrifices transmission rate and if strict delay-sensitive application is considered and/or coherence time is large, interleaving and coding might be difficult to employ [20].

Spatial diversity (or antenna diversity) technique refers to the deployment of multiple transmit and/or receive antennas, where the separation between adjacent antennas is larger than half of the carrier wavelength. Hence, received signals at different antennas will experience independent fading. Larger separation is required if shadowing effect is taken into consideration [18]. Receive diversity is obtained if multiple antennas are employed at the receiver, i.e., single-input multiple-output (SIMO). Transmit diversity refers to a multiple-input single-output (MISO) link where further details are given in the following section. Multiple-input multiple-output (MIMO) systems combine transmit and receive diversity.

Angle diversity is obtained by employing various directive antennas at the receiver taking advantage of uncorrelated scattered signals associated with the various directions [18]. In path diversity technique for direct sequence spread spectrum (DSSS) systems, the transmitted signal is sent over a bandwidth that is larger than channel coherence bandwidth. So-called Rake receiver is used to

separate received signal components from different propagation paths and then to combine them constructively [18], [19].

Components of independent faded received signals (obtained through one of the aforementioned diversity techniques) can be processed by different methods. For instance, maximal ratio combining (MRC) is applied under the assumption of perfect knowledge of amplitude and phase of fading channel at the receiver. Other linear combining schemes with reduced complexity such as equal-gain combining (EGC) and selective combining (SC) are available as well. MRC combining technique achieves the best performance among other combining schemes [18].

1.2.1 Transmit Diversity

Transmit diversity requires multiple antennas at transmitter performing pre-processing and pre-coding prior to transmission. There are two main implementations of transmit diversity based on the availability of channel state information (CSI) at the transmitter; namely, closed-loop and open loop transmit diversity. In closed-loop transmit diversity, CSI is assumed to be available both at the receiver and transmitter sides. This requires a feedback channel in practice. Open-loop transmit diversity technique on the other hand does not require prior knowledge of CSI at transmitter. In [21], Wittneben proposes a delay diversity scheme; an open-loop transmit diversity scheme which is considered as the ancestor to space-time codes of [2].

Space-time coding (STC) is a systematic treatment to encode signals at transmitter as an open-loop transmit diversity scheme. The primary criterion in STC design is to maximize diversity gain, which is the slope of performance curve at high signal-to-noise ratio. A diversity gain of $r \times N_R$ is obtained where r is the rank of the STC matrix and N_R is the number of antennas at receiver. For full rank code matrix, maximum diversity gain is achieved, i.e., $N_T \times N_R$, where N_T is the number of antennas at transmitter [22]. The secondary design criterion is maximizing coding gain, which can be attained by maximizing the minimum of $\prod_{m=1}^r \lambda_m$, where λ_m 's are related to eigenvalues of code matrix over all possible codeword pairs. This criterion is called determinant criterion [22].

There are several classes of space-time codes. One well-known category of STC is space-time block code (STBC). Alamouti in [23] introduces the first orthogonal STBC design using two transmit antennas. Extension of STBCs to multiple transmit antennas is presented by Tarokh et. al. in [24]

using theory of orthogonal designs based on the work of Randon and Hurwitz in this branch of mathematics [25]. Space-time trellis codes (STTC) are able to provide additional coding gains [2] besides the spatial diversity. Initial STTC designs are hand-made, but additional designs can be found in [26-29]. Other transmit diversity schemes include layered space-time (LST) coding such as Bell labs layered space-time (BLAST), diagonal layered space-time (DLST), threaded layered space-time (TLST) [30, 31], and linear dispersion codes (LDC) [32], [33].

1.2.2 Cooperative Diversity

Despite the promising data rate and/or low error rate achieved by STC in MIMO communication systems in fading channels, deployment of multiple antennas at transmitter and/or receiver might not be feasible in some applications due to limitation in size, power, and hardware complexity in end-user devices. Cooperative diversity has been proposed as a powerful alternative fading-mitigation technique [34-38]. Cooperative diversity takes advantage of the broadcast nature of wireless transmission where a transmitted signal can be overheard by many unintended nodes. If these unintended nodes (or relays) are willing to share their resources with the source node, they can together create a virtual antenna array to extract the spatial diversity in a distributed fashion. The concept of cooperative diversity can be traced back to Van der Meulen's earlier work [39] on relay channels. The recent surge of interest however has followed after the works of Laneman et al. and Sendonaris et al. [34, 35, 37, 38].

In [40], Sendonaris et. al. propose a cooperative scheme for in-cell mobile users which increase data rate and uplink capacity. This advantage in higher data rate can be sacrificed to reduce power consumption per user or extend cell coverage with the expense of extra complexity at receiver. In [41], Laneman and Wornell develop transmission protocols for amplify-and-forward (AF) and decode-and-forward (DF) relaying. In their cooperation scheme, transmission is carried in two phases; broadcasting and relaying phases. In the broadcasting phase, source node (or user) broadcasts its information to intended destination node (BS or another user) and other nodes, i.e., relay nodes, located within transmission range of source node. In relaying phase of AF scheme, nodes working as relays amplify the received information signal and forward it to the destination node. Hence, destination node receives two faded versions of information, i.e., from broadcasting and relaying phases. In DF scheme, broadcasting phase is identical to AF scheme however; in the relaying phase,

relay node decodes the received signal and then transmits it to destination node. Both schemes require knowledge of inter-user channel coefficients to perform optimal decoding.

For multi-relay deployment, Laneman et. al. [34, 35] consider two main approaches, space-time coded and repetition-based cooperative protocols. Repetition-based cooperative protocol provides full spatial diversity at the price of decreasing bandwidth efficiency as the number of cooperating nodes increases. In relaying phase, relay nodes operating under repetition-based scheme transmit information on orthogonal subchannels. Space-time coded cooperative protocol is an alternative methodology to attain full spatial diversity without sacrificing bandwidth efficiency. In relaying phase, relay nodes operating in space-time coded cooperative scheme will transmit simultaneously on the same subchannel [34].

After the work in [34, 35, 37, 38], a large number of publications have appeared in the area of cooperative communications investigating variety of topics such as information theoretic bounds, cooperation protocols, distributed space-time code design, distributed source coding, optimum power allocation, cross-layer design etc. among others. Detailed surveys of various issues in cooperative communication systems can be found in recent books [4], [5].

1.3 Research Motivation

The current rich literature on cooperative diversity is mainly limited to the conventional assumption of AWGN. Although AWGN model realistically represents the thermal noise at the receiver, it ignores the impulsive nature of noise, which might be dominant in various environments as earlier discussed in section 1.1. This has motivated several researchers to analyze the performance of communication systems in the presence of impulsive noise. In [42] and [43], Spaulding and Middleton have derived optimum coherent and non-coherent detection rules using maximum likelihood detection for fading and non-fading channels in the presence of impulsive noise. In [44], Haring and Vinck have investigated the performance of coded transmission over impulsive noise through the derivations of Chernoff factor and cut-off rate assuming a MAP (maximum a posteriori) detector. In [45], Tepedelenlioglu and Gao have studied the performance of various diversity reception techniques in impulsive noise. In particular, they have derived upper bounds on average bit error rate and investigated the performance of MRC, EGC, SC, and PDC (post-detection combining). In [46], they have extended their work to transmit diversity where they have obtained design criteria

for space-time codes. They have further investigated the performance of MIMO systems with different receiver types including genie-aided, MAP, and minimum distance receivers.

To the best of our knowledge, no research results have been published on cooperative diversity in the presence of impulsive noise. Aiming to fill this research gap, this thesis presents an error rate performance analysis of cooperative diversity over Rayleigh fading channel in impulsive noise. In particular, we consider a multi-relay system with AF relaying and assume space-time coded and repetition-based cooperative protocols [34, 35]. We obtain upper bounds on pairwise error probability (PEP) expression for these cooperative schemes under Middleton Class A noise, which includes Gaussian noise as a special case. Our results demonstrate that the performance of cooperative system highly depends on the impulsive nature of noise and different diversity orders dominate the performance in different ranges of signal-to-noise ratios (SNRs). We further optimize the bit error rate (BER) performance through proper power allocation among cooperating nodes. The optimization yields gains up to ~ 3 dB at a target BER of 10^{-6} in a highly impulsive environment for a two-relay cooperative scheme. In near-Gaussian impulsive environment, performance gains climb up to 5 dB depending on the relays' locations.

1.4 Thesis Outline

The rest of the thesis is organized as follows: In Chapter 2, we describe the system model introducing fading channel, noise model, and cooperative transmission model under consideration. In Chapter 3, we derive PEP expressions and obtain upper bounds on the error rate performance. We analyze diversity gains based on the derived PEP expressions. In Chapter 4, we optimize power allocation based on the minimization of union bound on BER for different impulsive environments. In Chapter 5, we present extensive Monte Carlo simulations for various impulsive environments. Conclusions are presented in Chapter 6.

Chapter 2

System Model

In this chapter, we introduce the cooperative transmission model under consideration along with fading channel and impulsive noise.

2.1 Fading Channel Model

In this thesis, we assume an aggregate channel model which takes into account both small-scale fading and large-scale path loss. In a multi-relay communication system as shown in Figure 2.1, the fading coefficients over source-to-destination ($S \rightarrow D$), source-to- i^{th} relay ($S \rightarrow R_i$), and i^{th} relay-to-destination ($R_i \rightarrow D$) links are respectively denoted by h_{SD} , h_{SR_i} , and h_{R_iD} , $i = 1, \dots, M$. They are assumed to be independent and identically distributed (i.i.d) zero-mean complex Gaussian random variables leading to a Rayleigh fading channel model.

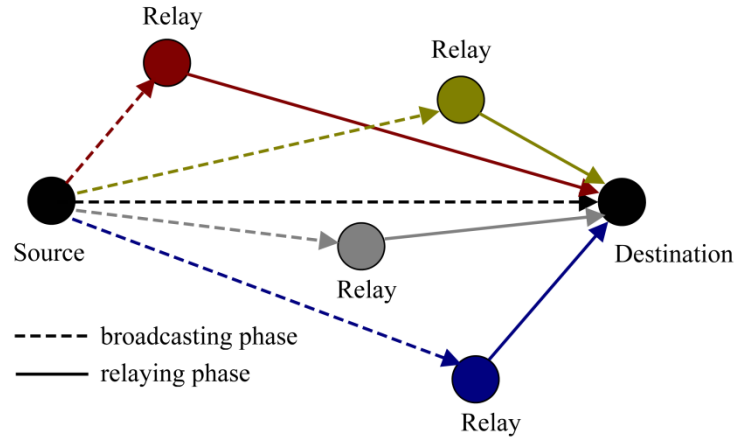


Figure 2.1: Relay-assisted transmission.

Path losses in $S \rightarrow D$, $S \rightarrow R_i$, and $R_i \rightarrow D$ are respectively denoted by $cd_{SD}^{-\alpha}$, $cd_{SR_i}^{-\alpha}$, and $cd_{R_iD}^{-\alpha}$ where d_{SD} , d_{SR_i} , and d_{R_iD} are the corresponding distances among nodes, α is path loss coefficient, and c is a constant related to propagation environment. We denote the angle formed by $S \rightarrow R_i$ and $R_i \rightarrow D$ links by φ_i . Normalizing the path losses with respect to the direct path, the relative

geometrical gains are defined as $g_{SR_i} = (d_{SR_i} / d_{SD})^{-\alpha}$ and $g_{R_iD} = (d_{R_iD} / d_{SD})^{-\alpha}$ [47]. They can be further related to each other through law of cosines, i.e., $g_{R_iD}^{2/\alpha} + g_{SR_i}^{2/\alpha} - 2g_{SR_i}^{1/\alpha} g_{R_iD}^{1/\alpha} \cos \varphi_i = g_{SR_i}^{2/\alpha} g_{R_iD}^{2/\alpha}$. Path loss ratio can be defined as

$$\Theta_i = \frac{g_{SR_i}}{g_{R_iD}} = \left(\frac{d_{R_iD}}{d_{SR_i}} \right)^\alpha \quad (2.1)$$

which indicates the relative location of i^{th} relay with respect to source and destination. If $\Theta_i < 0$ dB, then the relay is close to destination node. On the contrary, when $\Theta_i > 0$ dB, this indicates that relay is close to source node. For $\Theta_i = 0$ dB, the relay is located in the middle between source and destination.

2.2 Impulsive Noise Model

We assume Middleton Class A model to represent the impulsive noise under consideration. Noise at the receiver is given by

$$n_r = n_g + n_i \quad (2.2)$$

where n_g represents the thermal noise and is modeled by zero-mean complex-valued Gaussian with variance σ_g^2 . In (2.2), n_i is the impulsive component and results from the occurrence of interfering waveforms from active interfering sources. Under the assumption that the number of such sources is large enough and they emit independently, occurrence of interferences follow Poisson distribution [17]. Therefore, the probability of having k active interferences (or impulses) is denoted by α_k and given by

$$\alpha_k = \exp(-A) \frac{A^k}{k!} \quad (2.3)$$

where A is called the impulsive index and indicates the average number of impulses during interference time. Probability density function (pdf) of the complex-valued noise at receiver is given by

$$p(n_r) = \sum_{k=0}^{\infty} \frac{\alpha_k}{\pi \sigma_k^2} \exp\left(-\frac{|n_r|^2}{\sigma_k^2}\right) \quad (2.4)$$

where σ_k^2 is the conditional variance given that k impulses are affecting the receiver. It is calculated as

$$\sigma_k^2 = \sigma^2 \beta_k \quad (2.5)$$

where σ^2 denotes the mean variance of impulsive noise n_r and is equal to N_0 and β_k is given by

$$\beta_k = \left(\frac{kA^{-1} + \Gamma}{1 + \Gamma} \right) \quad (2.6)$$

In (2.6), Γ is the Gaussian factor which is the ratio between the variance of background Gaussian component σ_g^2 and the variance of the impulsive component σ_i^2 .

Middleton Class A model is therefore mainly characterized by two parameters, namely, impulsive index A , and Gaussian factor Γ . As A decreases, i.e., $A \rightarrow 0$, noise becomes highly structured and more impulsive. On the contrary, if A increases, i.e., $A \rightarrow \infty$, noise tends to Gaussian. Similarly, for small values of Γ , generated noise becomes more impulsive while it tends to Gaussian for large values of Γ . Probability density function of a real-valued random variable following Middleton Class A model with different values of A and Γ is depicted in Figure 2.2.

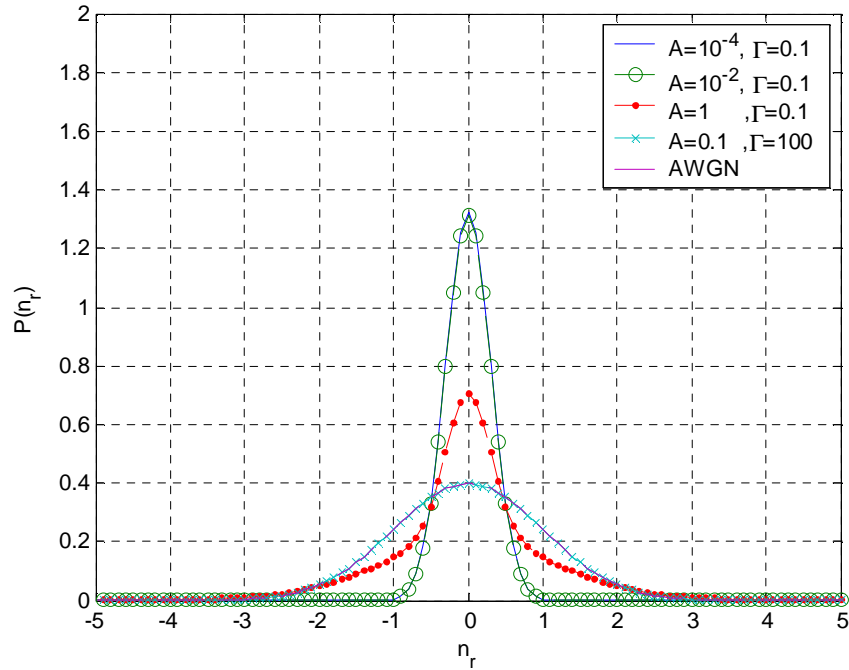


Figure 2.2: Probability density function of Middleton Class A model

In this thesis, we assume that impulsive noise samples are temporally dependent during a transmission frame. This is well justified through experimental observations on impulsive noise [48]. As for spatial dimension, we consider both dependent and independent impulsive noise. Spatially dependent is applicable when the same set of interfering sources affects destination and relay nodes together. In this case, destination and relay nodes observe relatively the same distance to the interfering sources [46]. On the other hand, spatially independent case occurs if different sets of interfering sources affect destination and relay nodes.

2.3 Transmission Model

We assume space-time coded and repetition-based cooperative protocols of [34], [36], which is the distributed SIMO (single-input multiple-output) implementation. During the broadcasting phase (i.e., P time slots), destination node D and relays R_1, \dots, R_M are in receive mode. The received signals corrupted by fading and impulsive noise are first normalized at relay nodes to ensure unity of average energy. Then either repetition coding or space-time block coding is applied across these signals before they are forwarded to the destination in relaying phase, which spans a duration of L time slots. Let E denote the average energy per time slot. Therefore, total energy consumed by source node S in broadcasting phase (of P time slots) is PE . On the other hand, in relaying phase (of L time slots), M relays consume a total energy of LE . Since we will deal with optimum power allocation in later sections, we also introduce the optimization parameters here. The first optimization parameter ξ determines the ratio of power allocated between broadcasting and relaying phases. On the other hand, optimization parameters $\psi_1, \dots, \psi_{M-1}$ are used to determine how the available relaying power is allocated among relay nodes.

2.3.1 Space-Time Coded Cooperative Diversity (STC-CD) Scheme

Let x_1, \dots, x_p denote M-PSK (phase shift keying) modulation signals to be transmitted. The received signals at destination node D and i^{th} relay R_i during p^{th} time slot of the broadcasting phase are given respectively by

$$r_{D,p} = \sqrt{\hat{\xi}E} h_{SD} x_p + n_{D,p}, \quad p = 1, \dots, P \quad (2.7)$$

$$r_{R_i,p} = \sqrt{g_{SR_i} \hat{\xi}E} h_{SR_i} x_p + n_{R_i,p} \quad (2.8)$$

where $\hat{\xi} = ((P+L)/P)\xi$. In (2.7)-(2.8) $n_{R_i,p}$ and $n_{D,p}$ represent the impulsive noise terms at relay and destination nodes. After proper scaling at relay nodes [36], [47], the received signals are applied to a space-time block encoder [34].

We assume that space-time block codes (STBCs) of [24] are employed across relay terminals. Let \mathbf{Y} denote the space-time code matrix with size of $M \times L$ which consists of elements as linear functions of $x_{i,1}, \dots, x_{i,L}$ and/or $x_{i,1}^*, \dots, x_{i,L}^*$. Further, let \mathbf{N} denote the $M \times L$ matrix for impulsive noise samples at relays. The received signal at destination during $(P+l)^{th}$ time slot is

$$r_{D,P+l} = \boldsymbol{\mu} \mathbf{y}_l + \boldsymbol{\lambda} \mathbf{n}_l + n_{D,P+l}, \quad l = 1, \dots, L \quad (2.9)$$

where \mathbf{y}_l is the l^{th} column vector of \mathbf{Y} , \mathbf{n}_l is the l^{th} column vector of \mathbf{N} such that i^{th} element of $\mathbf{n}_l \in \{n_{R_i,P+l}, -n_{R_i,P+l}, n_{R_i,P+l}^*, -n_{R_i,P+l}^*\}$ based on the form of code matrix \mathbf{Y} . In (2.9), $\boldsymbol{\mu}$ and $\boldsymbol{\lambda}$ are defined as

$$\boldsymbol{\mu} = \left[\varepsilon_1 h_{SR_1}^{(*)} h_{R_1D} \quad \cdots \quad \varepsilon_M h_{SR_M}^{(*)} h_{R_MD} \right]_{1 \times M} \quad (2.10)$$

$$\boldsymbol{\lambda} = \left[v_1 h_{R_1D} \quad \cdots \quad v_M h_{R_MD} \right]_{1 \times M} \quad (2.11)$$

where $h_{SR_i}^{(*)} \in \{h_{SR_i}, h_{SR_i}^*\}$ and ε_i and v_i are given by

$$\varepsilon_i = \sqrt{\left(\hat{\psi}_i g_{SR_i} g_{R_iD} \hat{\xi} (1-\xi) E^2 \right) / \left(g_{SR_i} \hat{\xi} E + N_0 \right)} \quad (2.12)$$

$$v_i = \sqrt{\left(\hat{\psi}_i g_{R_iD} (1-\xi) E \right) / \left(g_{SR_i} \hat{\xi} E + N_0 \right)} \quad (2.13)$$

with

$$\hat{\psi}_i = \begin{cases} ((P+L)/L) \psi_i, & i = 1, \dots, M-1 \\ ((P+L)/L) \left(1 - \sum_{i=1}^{M-1} \psi_i \right), & i = M \end{cases} \quad (2.14)$$

The received signals at destination node are normalized by $\Omega = \sqrt{1 + \sum_{i=1}^M v_i^2}$ [36] which yields

$$\tilde{r}_{D,P+l} = \tilde{\boldsymbol{\mu}} \mathbf{y}_l + \tilde{\mathbf{n}}_{D,P+l}, \quad l = 1, \dots, L \quad (2.15)$$

where we define $\tilde{r}_{D,P+l} = r_{D,P+l} / \Omega$, $\tilde{\boldsymbol{\mu}} = \boldsymbol{\mu} / \Omega$, and $\tilde{\mathbf{n}}_{D,P+l} = (\boldsymbol{\lambda} \mathbf{n}_l + n_{D,P+l}) / \Omega$. To introduce a compact matrix form representation, we further define

$$\mathbf{r} = \left[r_{D,1} \quad \cdots \quad r_{D,P} \quad \tilde{r}_{D,P+1} \quad \cdots \quad \tilde{r}_{D,P+L} \right]_{1 \times (P+L)} \quad (2.16)$$

$$\mathbf{h} = \left[\sqrt{\hat{\xi}} E h_{SD} \cdots \sqrt{\hat{\xi}} E h_{SD} \quad \tilde{\boldsymbol{\mu}} \right]_{1 \times (P+M)} \quad (2.17)$$

$$\mathbf{n} = \left[n_{D,1} \quad \cdots \quad n_{D,P} \quad \tilde{n}_{D,P+1} \quad \cdots \quad \tilde{n}_{D,P+L} \right]_{1 \times (P+L)} \quad (2.18)$$

$$\mathbf{X} = \left[\mathbf{x}_1 \quad \mathbf{x}_2 \right]_{(P+M) \times (P+L)} \quad (2.19)$$

where $\mathbf{x}_1 = [\text{diag}(x_1, \dots, x_P) \quad \mathbf{0}]^T$ and $\mathbf{x}_2 = [\mathbf{0} \quad \mathbf{Y}]^T$. Then we have

$$\mathbf{r} = \mathbf{h} \mathbf{X} + \mathbf{n} \quad (2.20)$$

which describes the received signal for the transmission frame of $P+L$ slots.

2.3.2 Repetition-based Cooperative Diversity (RB-CD) Scheme

In RB-CD scheme, signals at the relaying phase are transmitted through orthogonal subchannels [34]. In this case, the received signal still takes the form of (2.20) where \mathbf{r} , \mathbf{h} , \mathbf{n} and \mathbf{X} are now defined as

$$\mathbf{r} = \left[r_{D,1} \quad \cdots \quad r_{D,P} \quad r_{D,P+1} \quad \cdots \quad r_{D,P(M+1)} \right]_{1 \times P(M+1)} \quad (2.21)$$

$$\mathbf{h} = \left[\sqrt{\hat{\xi}} E h_{SD} \quad \cdots \quad \sqrt{\hat{\xi}} E h_{SD} \quad \tilde{\boldsymbol{\mu}} \quad \cdots \quad \tilde{\boldsymbol{\mu}} \right]_{1 \times P(M+1)} \quad (2.22)$$

$$\mathbf{n} = \left[n_{D,1} \cdots n_{D,P} \quad \tilde{n}_{D,P+1} \quad \cdots \quad \tilde{n}_{P(M+1)} \right]_{1 \times P(M+1)} \quad (2.23)$$

$$\mathbf{X} = \text{diag}(x_1, \dots, x_P, x_1, \dots, x_1, \dots, x_P, \dots, x_P)_{P(M+1) \times P(M+1)} \quad (2.24)$$

with $\boldsymbol{\mu} = [\varepsilon_1 h_{SR_1} h_{R_1 D} \cdots \varepsilon_M h_{SR_M} h_{R_M D}]$, $\tilde{n}_{D,P+l} = (\lambda_n n_{R_n,l} + n_{D,P+l}) / \Omega_n$, $\tilde{\boldsymbol{\mu}}_i = \boldsymbol{\mu}_i / \Omega_i$ and $\Omega_i = \sqrt{1 + v_i^2}$, $i \in \{1, \dots, M\}$, $n = l + M(1 - \lceil l/M \rceil)$ and $l \in \{1, \dots, PM\}$. The received signal is then fed to a minimum distance receiver as in STC-CD scheme.

2.4 Receiver

The received signal is fed to a minimum distance receiver (MDR) [46]

$$\hat{\mathbf{X}} = \min_{\mathbf{X}} \|\mathbf{r} - \mathbf{h} \mathbf{X}\|^2 \quad (2.25)$$

Although MDR is not optimal for impulsive noise environment, we use it as a practical low-complexity detection technique. The optimal detector for impulsive noise requires estimation of

interference distribution, non-linear processing and adaptive receivers capable of adjusting parameters related to interference [42, 43]. Further discussions on various types of receivers for impulsive noise can be found in [46].

Chapter 3

Error Rate Performance Analysis

In this chapter, we are interested in obtaining bounds on the error rate performance. We first derive the pairwise error probability (PEP) which constitutes the building block for the derivation of union bounds to the error probability. Let \mathbf{X} and $\widehat{\mathbf{X}}$ denote, respectively, the original transmitted codeword and decoded codeword. In our derivations, we consider both cases of spatially dependent and independent noise at destination and relay nodes. In both cases, noise samples are assumed to be temporally dependent during transmission frame.

3.1 Performance of STC-CD Scheme

Considering the transmission model in subsection 2.3.1 for STC-CD scheme, we derive an upper bound on the performance of this system. The Euclidean distance between \mathbf{X} and $\widehat{\mathbf{X}}$ conditioned on fading coefficients is given by

$$d^2(\mathbf{X}, \widehat{\mathbf{X}}) = \mathbf{h}(\mathbf{X} - \widehat{\mathbf{X}})(\mathbf{X} - \widehat{\mathbf{X}})^H \mathbf{h}^H \quad (3.1)$$

3.1.1 PEP for Spatially Dependent Noise

In spatially dependent case, we assume that the number of impulses affecting relays R_1, \dots, R_M and destination node D is identical and denoted by Poisson random variable C . Considering all possible realizations of C , the conditional PEP is given by

$$P(\mathbf{X}, \widehat{\mathbf{X}} | \mathbf{h}) = \sum_{k=0}^{\infty} \alpha_k Q \left(\sqrt{\frac{d^2(\mathbf{X}, \widehat{\mathbf{X}})}{2\beta_k N_0}} \right) \quad (3.2)$$

where α_k and β_k can be calculated through (2.3) and (2.6). Using Chernoff upper bound in (3.2), conditional PEP is given by

$$P(\mathbf{X}, \widehat{\mathbf{X}} | \mathbf{h}) \leq \sum_{k=0}^{\infty} \alpha_k \exp\left(-d^2(\mathbf{X}, \widehat{\mathbf{X}})/4\beta_k N_0\right) \quad (3.3)$$

Exact PEP and Chernoff bound expressions, which can be evaluated by taking expectation over fading coefficients \mathbf{h} , respectively are

$$P(\mathbf{X}, \widehat{\mathbf{X}}) = E_h \left[\sum_{k=0}^{\infty} \alpha_k Q \left(\sqrt{\frac{d^2(\mathbf{X}, \widehat{\mathbf{X}})}{2\beta_k N_0}} \right) \right] \quad (3.4)$$

$$P(\mathbf{X}, \widehat{\mathbf{X}}) \leq E_h \left[\sum_{k=0}^{\infty} \alpha_k \exp\left(-d^2(\mathbf{X}, \widehat{\mathbf{X}})/4\beta_k N_0\right) \right] \quad (3.5)$$

Taking expectation with respect to fading coefficients $|h_{SD}|^2, |h_{SR_1}|^2, \dots, |h_{SR_M}|^2$, which follow exponential distribution, the conditional PEP can be obtained as

$$P(\mathbf{X}, \widehat{\mathbf{X}} \mid |h_{R_1D}|^2, \dots, |h_{R_MD}|^2) \leq \int_0^{\infty} \dots \int_0^{\infty} \left(\sum_{k=0}^{\infty} \alpha_k \exp\left(-d^2(\mathbf{X}, \widehat{\mathbf{X}})/4\beta_k N_0\right) \right) \times f_{|h_{SD}|^2}(t_1) f_{|h_{SR_1}|^2}(t_2) \dots f_{|h_{SR_M}|^2}(t_{M+1}) dt_1 dt_2 \dots dt_{M+1} \quad (3.6)$$

$$= \sum_{k=0}^{\infty} \alpha_k \left(1 + \frac{\widehat{\xi} \Delta E}{4\beta_k N_0} \right)^{-1} \prod_{m=1}^M \left(1 + \frac{\eta_m \varepsilon_m^2 |h_{R_mD}|^2 E}{4\beta_k N_0 \Omega^2} \right)^{-1} \quad (3.7)$$

where $\Delta = \sum_{i=1}^P |x_i - \widehat{x}_i|^2$, η_m 's are the eigenvalues of STBC code matrix \mathbf{Y} , and $f_{|h_{SD}|^2}(\cdot)$ denotes the pdf of $|h_{SD}|^2$. Further, taking expectation with respect to $|h_{R_1D}|^2, \dots, |h_{R_MD}|^2$, which also follow exponential distribution, the unconditional PEP is obtained as

$$P(\mathbf{X}, \widehat{\mathbf{X}}) \leq \sum_{k=0}^{\infty} \alpha_k \left(1 + \frac{\widehat{\xi} \Delta E}{4\beta_k N_0} \right)^{-1} \prod_{m=1}^M \left(\frac{\eta_m \varepsilon_m^2 E}{4\beta_k \Omega^2 N_0} \right)^{-1} \exp\left(\frac{4\beta_k \Omega^2}{\eta_m \varepsilon_m^2 (E/N_0)} \right) \times \Gamma\left(0, \frac{4\beta_k \Omega^2}{\eta_m \varepsilon_m^2 (E/N_0)} \right) \quad (3.8)$$

where $\Gamma(\cdot, \cdot)$ is the upper incomplete Gamma function [49]. The infinite summation in the derived PEP expression can be safely truncated to a finite summation without significant loss because probability of very large number of interferences is negligible and Poisson distribution approaches zero for large value of impulses. To verify the accuracy of derived PEP expression, (3.8) is plotted along with the exact PEP given by (3.4) and Chernoff bound given by (3.5). We consider both highly impulsive (HI) and near-Gaussian (NG) channels. As expected, (3.5) and (3.8) coincide for both cases.

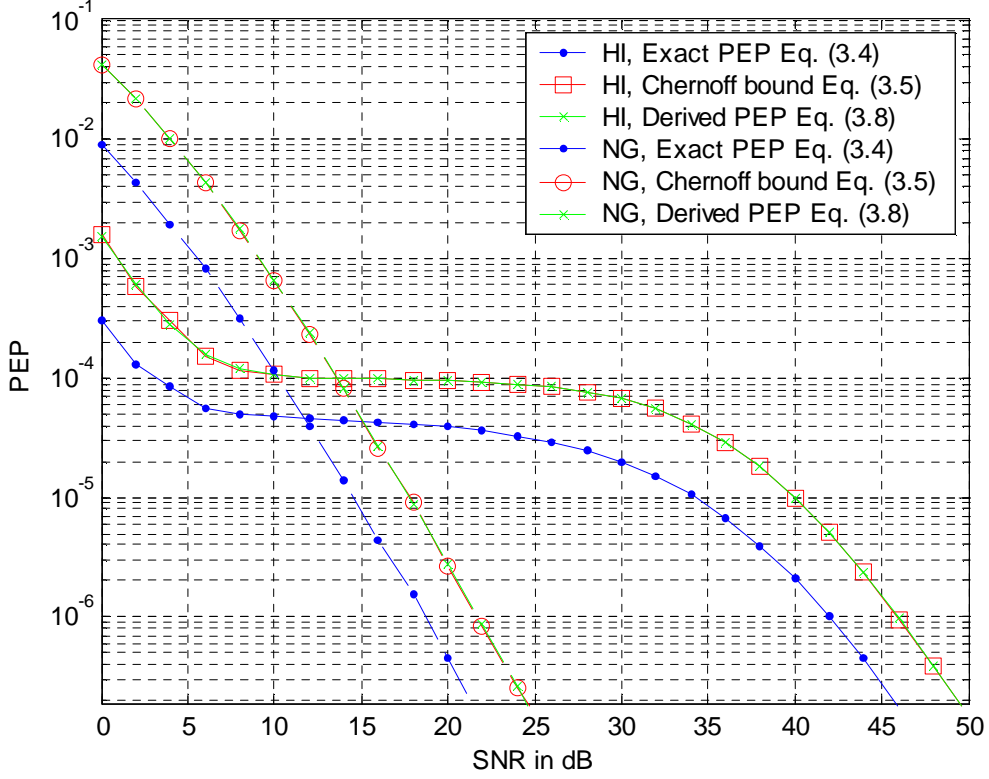


Figure 3.1: Comparison of derived PEP expression and Chernoff bound of STC-CD scheme in spatially dependent noise.

We also note that the derived PEP expression includes the conventional Gaussian assumption as a special case. Recall that conditional variances of impulsive noise is given by $\beta_k N_0$. As $\Gamma \rightarrow \infty$, β_k converges to one. The summation of α_k in (3.8) over all possible values of k becomes equal to one. Consequently, PEP expression reduces to

$$\begin{aligned}
 P(\mathbf{X}, \hat{\mathbf{X}}) &\leq \left(1 + \frac{\hat{\xi} \Delta E}{4N_0}\right)^{-1} \prod_{m=1}^M \left(\frac{\eta_m \varepsilon_m^2 (E/N_0)}{4\Omega^2}\right)^{-1} \exp\left(\frac{4\Omega^2}{\eta_m \varepsilon_m^2 (E/N_0)}\right) \\
 &\quad \times \Gamma\left(0, \frac{4\Omega^2}{\eta_m \varepsilon_m^2 (E/N_0)}\right)
 \end{aligned} \tag{3.9}$$

which is the PEP expression for AWGN case.

3.1.2 PEP for Spatially Independent Noise

Now, we return our attention to the case where we have spatially independent noise samples. Assume that number of impulses affecting relays R_1, \dots, R_M are statistically independent and denoted by Poisson random variables C_1, \dots, C_M . On the other hand, C_{M+1} is a Poisson random variable representing the number of impulses affecting destination node D . Contrary to single summation expression for spatially dependent case, the conditional PEP is now given by

$$P(\mathbf{X}, \widehat{\mathbf{X}} | \mathbf{h}) = \sum_{k_1=0}^{\infty} \dots \sum_{k_i=0}^{\infty} \dots \sum_{k_{M+1}=0}^{\infty} \left(\prod_{n=1}^{M+1} \alpha_{k_n} \right) \times Q \left(d^2(\mathbf{X}, \widehat{\mathbf{X}}) / \sqrt{2 \left(\widehat{\xi} |h_{SD}|^2 \Delta E \beta_{k_{M+1}} + \sum_{m=1}^M \eta_m (\varepsilon_m^2 / \Omega^2) |h_{SR_m}|^2 |h_{R_mD}|^2 \beta_{k_m} \right) N_0} \right) \quad (3.10)$$

Exact PEP expression can be evaluated by taking expectation over fading coefficients \mathbf{h} of conditional PEP expression in (3.10). An approximation of the conditional PEP expression can be obtained as

$$P(\mathbf{X}, \widehat{\mathbf{X}} | \mathbf{h}) \approx \sum_{k_1=0}^{\infty} \dots \sum_{k_i=0}^{\infty} \dots \sum_{k_{M+1}=0}^{\infty} \left(\prod_{n=1}^{M+1} \alpha_{k_n} \right) \times Q \left(\sqrt{\left[\widehat{\xi} |h_{SD}|^2 \Delta E + \sum_{m=1}^M \eta_m (\varepsilon_m^2 / \Omega^2) |h_{SR_m}|^2 |h_{R_mD}|^2 \right] / 2\Phi N_0} \right) \quad (3.11)$$

by setting $\beta_{k_1} = \dots = \beta_{k_{M+1}} = \Phi$, which denotes the average number of impulses affecting the destination and relay nodes during a transmission frame and is given by

$$\Phi = (L \sum_{m=1}^M \beta_{k_m} + (P+L) \beta_{k_{M+1}}) / ((M+1)L + P) \quad (3.12)$$

Using Chernoff upper bound and taking expectations with respect to fading coefficients, we obtain

$$P(\mathbf{X}, \widehat{\mathbf{X}}) \lesssim \sum_{k_1=0}^{\infty} \dots \sum_{k_i=0}^{\infty} \dots \sum_{k_{M+1}=0}^{\infty} \left(\prod_{n=1}^{M+1} \alpha_{k_n} \right) \left(1 + \frac{\widehat{\xi} \Delta E}{4\Phi N_0} \right)^{-1} \prod_{m=1}^M \left(\frac{\eta_m \varepsilon_m^2 (E / N_0)}{4\Phi \Omega^2} \right)^{-1} \times \exp \left(\frac{4\Phi \Omega^2}{\eta_m \varepsilon_m^2 (E / N_0)} \right) \Gamma \left(0, \frac{4\Phi \Omega^2}{\eta_m \varepsilon_m^2 (E / N_0)} \right) \quad (3.13)$$

As justification for derived approximate PEP for STC-CD scheme in spatially independent noise, Chernoff bound and derived PEP expressions along with the exact PEP are illustrated in Figure 3.2. The approximate PEP provides a good match to the Chernoff bound in both HI and NG noise.

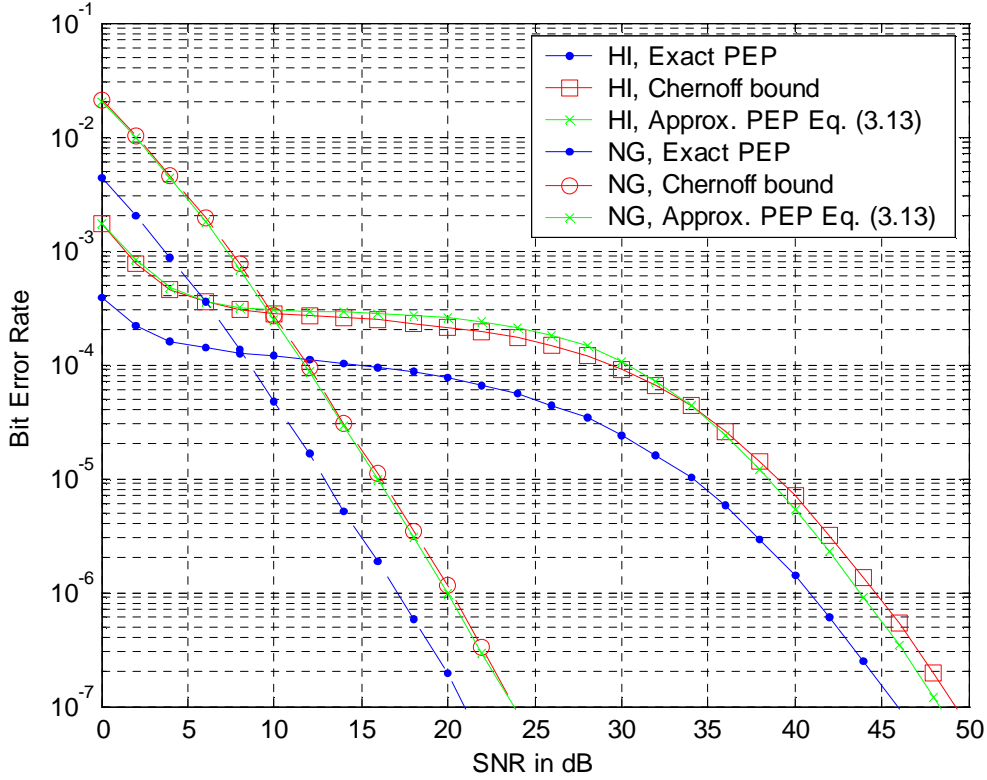


Figure 3.2: Comparison of derived PEP expression and Chernoff bound of STC-CD scheme in spatially independent noise.

3.2 Performance of RB-CD Scheme

3.2.1 PEP for Spatially Dependent Noise

The Euclidean distance between \mathbf{X} and $\widehat{\mathbf{X}}$ conditioned on fading coefficients is given by (3.1) where \mathbf{X} is now defined as in (2.24). In a similar manner to the derivations followed in section 3.1, taking expectation with respect to fading coefficients $|h_{SD}|^2, |h_{SR_1}|^2, \dots, |h_{SR_M}|^2$, the conditional PEP can be obtained as

$$P(\mathbf{X}, \widehat{\mathbf{X}} \mid |h_{R_1D}|^2, \dots, |h_{R_MD}|^2) \leq \sum_{k=0}^{\infty} \alpha_k \left(1 + \frac{\widehat{\xi} \Delta E}{4\beta_k N_0} \right)^{-1} \prod_{m=1}^M \left(1 + \frac{\Delta \varepsilon_m^2 |h_{R_mD}|^2 E}{4\beta_k N_0 (1 + \nu_m^2)} \right)^{-1} \quad (3.14)$$

Further, taking expectation with respect to $|h_{R_1D}|^2, \dots, |h_{R_M D}|^2$, which also follow exponential distribution, the unconditional PEP is obtained as

$$P(\mathbf{X}, \hat{\mathbf{X}}) \leq \sum_{k=0}^{\infty} \alpha_k \left(1 + \frac{\hat{\xi} \Delta E}{4\beta_k N_0} \right)^{-1} \prod_{m=1}^M \left(\frac{\Delta \varepsilon_m^2 (E/N_0)}{4\beta_k (1+v_m^2)} \right)^{-1} \exp \left(\frac{4\beta_k (1+v_m^2)}{\Delta \varepsilon_m^2 (E/N_0)} \right) \times \Gamma \left(0, \frac{4\beta_k (1+v_m^2)}{\Delta \varepsilon_m^2 (E/N_0)} \right) \quad (3.15)$$

The derived PEP expression along with the Chernoff bound and exact PEP expressions are illustrated in Figure 3.3.

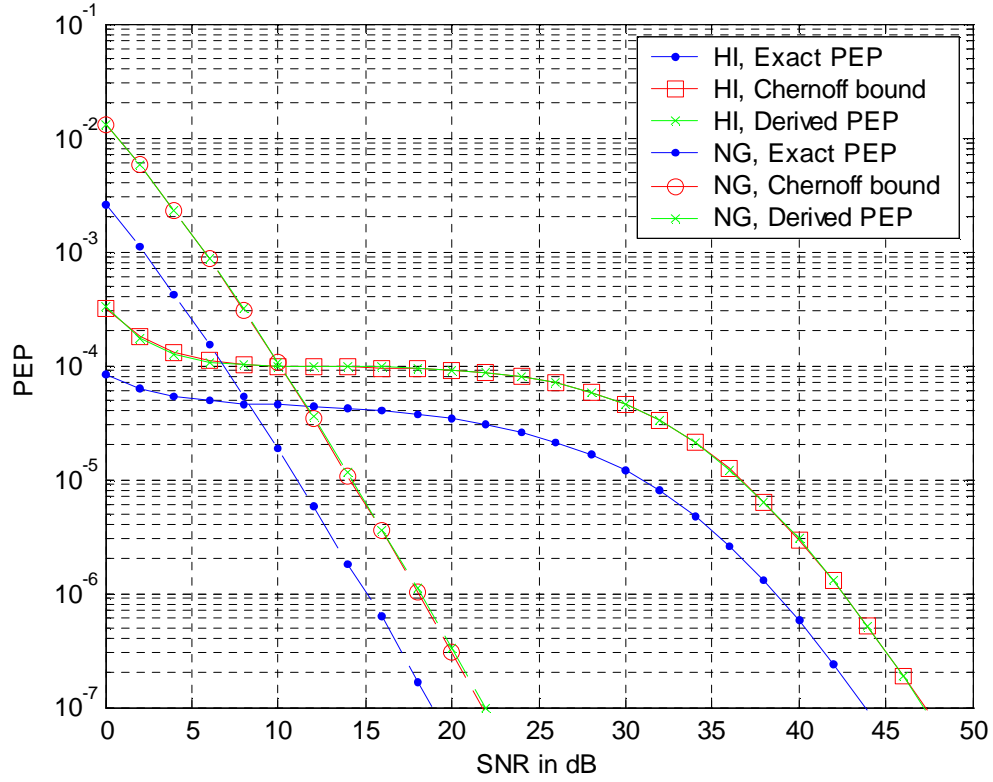


Figure 3.3: Comparison of derived PEP expression and Chernoff bound of RB-CD scheme in spatially dependent noise.

3.2.2 PEP for Spatially Independent Noise

Similar to derivation in subsection 3.1.2, the conditional PEP is given by

$$P(\mathbf{X}, \widehat{\mathbf{X}} | \mathbf{h}) = \sum_{k_1=0}^{\infty} \dots \sum_{k_i=0}^{\infty} \dots \sum_{k_{M+1}=0}^{\infty} \left(\prod_{n=1}^{M+1} \alpha_{k_n} \right) \times Q \left(d^2(\mathbf{X}, \widehat{\mathbf{X}}) / \sqrt{2 \left(\widehat{\xi} |h_{SD}|^2 \Delta E \beta_{k_{M+1}} + \sum_{m=1}^M \Delta(\varepsilon_m^2 / (1 + \nu_m^2)) |h_{SR_m}|^2 |h_{R_m D}|^2 \beta_{k_m} \right) N_0} \right) \quad (3.16)$$

An approximation of the conditional PEP expression can be obtained as

$$P(\mathbf{X}, \widehat{\mathbf{X}} | \mathbf{h}) \approx \sum_{k_1=0}^{\infty} \dots \sum_{k_i=0}^{\infty} \dots \sum_{k_{M+1}=0}^{\infty} \left(\prod_{n=1}^{M+1} \alpha_{k_n} \right) \times Q \left(\sqrt{\left[\widehat{\xi} |h_{SD}|^2 \Delta E + \sum_{m=1}^M \Delta(\varepsilon_m^2 / (1 + \nu_m^2)) |h_{SR_m}|^2 |h_{R_m D}|^2 \right] / 2\widetilde{\Phi} N_0} \right) \quad (3.17)$$

by setting $\beta_{k_1} = \dots = \beta_{k_{M+1}} = \widetilde{\Phi}$, which denotes the average number of impulses affecting the destination and relay nodes during a transmission frame and is given by

$$\widetilde{\Phi} = (P \sum_{m=1}^M \beta_{k_m} + P(M+1) \beta_{k_{M+1}}) / (P(1+2M)) \quad (3.18)$$

Taking expectations with respect to fading coefficients, we obtain the approximate PEP as

$$P(\mathbf{X}, \widehat{\mathbf{X}}) \lesssim \sum_{k_1=0}^{\infty} \dots \sum_{k_i=0}^{\infty} \dots \sum_{k_{M+1}=0}^{\infty} \left(\prod_{n=1}^{M+1} \alpha_{k_n} \right) \left(1 + \frac{\widehat{\xi} \Delta E}{4\widetilde{\Phi} N_0} \right)^{-1} \prod_{m=1}^M \left(\frac{\Delta \varepsilon_m^2 (E / N_0)}{4\widetilde{\Phi} (1 + \nu_m^2)} \right)^{-1} \times \exp \left(\frac{4\widetilde{\Phi} (1 + \nu_m^2)}{\Delta \varepsilon_m^2 (E / N_0)} \right) \Gamma \left(0, \frac{4\widetilde{\Phi} (1 + \nu_m^2)}{\Delta \varepsilon_m^2 (E / N_0)} \right) \quad (3.19)$$

The derived PEP expression along with the Chernoff bound and exact PEP expressions are illustrated in Figure 3.4.

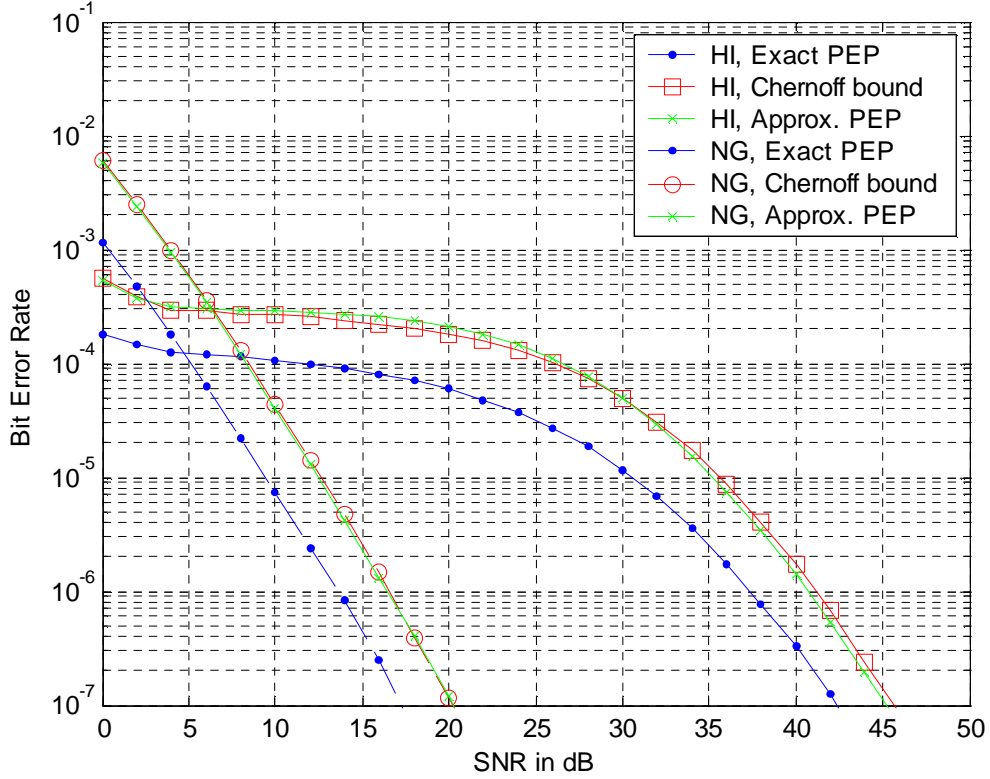


Figure 3.4: Comparison of derived PEP expression and Chernoff bound of RB-CD scheme in spatially independent noise.

3.3 Diversity Gain Analysis

Diversity gain is an essential parameter to quantify the enhancement of the wireless communication system deploying a diversity technique. In diversity gain analysis, we will discuss the achievable diversity order based on the derived PEP expressions in (3.9), (3.13), (3.15), and (3.19). Diversity order for finite SNR values is defined as [50]

$$d(E/N_0) = -\left(\frac{E}{N_0}\right) \left(\frac{\partial \log P(\mathbf{X} \rightarrow \widehat{\mathbf{X}})}{\partial (E/N_0)} \right) \quad (3.20)$$

Diversity order for STC-CD scheme is found as

$$d(E/N_0) = -\left(\frac{E/N_0}{P(\mathbf{X}, \widehat{\mathbf{X}})} \right) \sum_{k=0}^{\infty} \alpha_k A_0 [A_1 + A_2 + A_3 + A_4] \quad (3.21)$$

where A_0 , A_1 , A_2 , A_3 and A_4 are given by

$$A_0 = \left(1 + \frac{\hat{\xi}\Delta}{4\beta_k} (E/N_0)\right)^{-1} \left(\beta_k^M \left(\prod_{m=1}^M \left(\frac{\eta_m \alpha_m^2}{4\Omega^2}\right)\right)^{-1}\right) (E/N_0)^{-M} \times \exp\left((E/N_0)^{-1} \beta_k \sum_{m=1}^M \left(\frac{\eta_m \alpha_m^2}{4\Omega^2}\right)^{-1}\right) \left(\prod_{m=1}^M \Gamma_m\left(0, \frac{4\Omega^2 \beta_k}{\eta_m \alpha_m^2} (E/N_0)^{-1}\right)\right), \quad (3.22)$$

$$A_1 = \sum_{m=1}^M \left((E/N_0)^{-1} \exp\left(-\frac{4\Omega^2 \beta_k}{\eta_m \epsilon_m^2} (E/N_0)^{-1}\right) \left(\Gamma_m\left(0, \frac{4\Omega^2 \beta_k}{\eta_m \epsilon_m^2} (E/N_0)^{-1}\right)\right)^{-1} \right), \quad (3.23)$$

$$A_2 = -\beta_k (E/N_0)^{-2} \left(\sum_{m=1}^M \left(\frac{\eta_m \epsilon_m^2}{4\Omega^2}\right)^{-1}\right), \quad (3.24)$$

$$A_3 = -M (E/N_0)^{-1}, \quad (3.25)$$

$$A_4 = -\left(\frac{\hat{\xi}\Delta}{4\beta_k + \hat{\xi}\Delta(E/N_0)}\right). \quad (3.26)$$

In low SNR region, i.e., $E/N_0 \rightarrow 0$, an approximation of diversity order can be obtained as

$$d \cong -[A_1 + A_2 + A_3 + A_4] \quad (3.27)$$

where A_1 , A_2 , A_3 and A_4 are defined in (3.23)-(3.26) with replacing β_k by β_0 .

For high SNR values, i.e., $E/N_0 > 30$ dB, an approximation of diversity order can be given as

$$d \cong -(E/N_0)[A_1 + A_2 + A_3 + A_4] \quad (3.28)$$

where A_1 , A_2 , A_3 and A_4 are now calculated by replacing β_k in (3.23)-(3.26) by β_1 . For the limiting case of $E/N_0 \rightarrow \infty$, it can be shown that A_1 and A_2 converge to zero. Replacing those in (3.28), we observe that the diversity order converges to $M+1$ which is the full spatial diversity for the M -relay system under consideration. Details of this derivation are provided in Appendix.

3.4 Union Bound on BER Performance

Once PEP is obtained, we can obtain a union bound on the bit error rate (BER) using [51]

$$P_b \leq \frac{1}{n} \sum_{\mathbf{X}} p(\mathbf{X}) \sum_{\mathbf{X} \neq \hat{\mathbf{X}}} q(\mathbf{X}, \hat{\mathbf{X}}) P(\mathbf{X}, \hat{\mathbf{X}}) \quad (3.29)$$

where $p(\mathbf{X})$ is the probability that codeword \mathbf{X} is transmitted, $q(\mathbf{X}, \widehat{\mathbf{X}})$ is the number of information bits in error if decoder decides in favor of $\widehat{\mathbf{X}}$, and n is the number of information bits per transmission. For example, union bounds on BER using BPSK, 4-PSK, and 8-PSK modulation schemes with Gray mapping respectively for RB-CD and STC-CD schemes are

$$P_{b,BPSK} \leq \Psi(4) + \Psi(8) \quad (3.30)$$

$$P_{b,QPSK} \leq \Psi(2) + 3\Psi(4) + 3\Psi(6) + \Psi(8) \quad (3.31)$$

$$\begin{aligned} P_{b,8PSK} \leq & \frac{2}{3}\Psi(0.5858) + \frac{4}{3}\Psi(2) + \frac{4}{3}\Psi(3.4142) + \frac{22}{3}\Psi(4) \\ & + \frac{4}{3}\Psi(1.1716) + 4\Psi(2.5858) + 2\Psi(4.5858) + \frac{16}{3}\Psi(5.4142) \\ & + \frac{8}{3}\Psi(6) + \frac{8}{3}\Psi(6.8284) + \frac{8}{3}\Psi(7.4142) + \frac{2}{3}\Psi(8) \end{aligned} \quad (3.32)$$

where we use $\Psi(\Delta)$ to denote the derived PEP expressions with Euclidean distance

$$\Delta = |x_1 - \widehat{x}_1|^2 + |x_2 - \widehat{x}_2|^2.$$

These expressions will be used in the next chapter in the formulation of the power allocation problem.

Chapter 4

Optimum Power Allocation

Optimum power allocation is a key technique to realize the full potentials of relay-assisted transmission promised by the information-theoretic results. In this chapter, we formulate and solve the optimum power allocation problem for STC-CD and RB-CD schemes under consideration aiming to minimize the BER performance.

4.1 Optimization of Power Allocation for Multi-Relay System

Optimization of power allocation is based on minimizing the union bound on BER with respect to $\xi, \psi_1, \dots, \psi_{M-1}$ which have been earlier defined in section 2.3 subject to constraints $0 \leq \xi, \psi_1, \dots, \psi_{M-1} \leq 1$. The minimization problem can be formulated as

$$\min_{0 \leq \xi, \psi_1, \dots, \psi_{M-1} \leq 1} \Lambda(\xi, \psi_1, \dots, \psi_{M-1}) \quad (4.1)$$

where $\Lambda(\xi, \psi_1, \dots, \psi_{M-1})$ is the objective function given by (3.29). Its specific form depends on the modulation scheme and coding employed across the relay terminals as discussed in section 3.4. Optimum values for power allocation in cooperative communication system are obtained by solving (4.1). A closed-form solution for (4.1) is unfortunately not available; however, this problem can be efficiently solved through numerical methods. We use MATLAB software to solve the optimization problem. Specifically we use the MATLAB function “fmincon” which is based on gradient-based method and employs sequential quadratic programming (SQP). At each iteration, a quadratic programming sub-problem is solved and an estimate of the Hessian of the Lagrangian is updated using Broyden, Fletcher, Goldfarb, and Shanno (BFGS) quasi-Newton method [52].

4.2 Numerical Results

In Tables 4-1, 4-2, 4-3, and 4-4, we report optimization values through numerical optimization for a two-relay system in HI and NG environments considering STC-CD and RB-CD schemes. We consider six representative scenarios where we have distinct geometrical layouts for two relays:

- Scenario 1: $\Theta_1 = -30$ dB, $\Theta_2 = -30$ dB ,
- Scenario 2: $\Theta_1 = 0$ dB, $\Theta_2 = -30$ dB ,

- Scenario 3: $\Theta_1 = 30$ dB, $\Theta_2 = -30$ dB ,
- Scenario 4: $\Theta_1 = 0$ dB, $\Theta_2 = 0$ dB ,
- Scenario 5: $\Theta_1 = 0$ dB, $\Theta_2 = 30$ dB ,
- Scenario 6: $\Theta_1 = 30$ dB, $\Theta_2 = 30$ dB .

4.2.1 Highly Impulsive (HI) Noise

First, we consider STC-CD scheme in HI noise, where we use Alamouti-coding across relays, 4-PSK modulation scheme, $\varphi_1 = \varphi_2 = \pi$, $A = 10^{-4}$, and $\Gamma = 0.1$. The optimization values are reported in Table 4-1¹ and it is observed that these values differ significantly from [47] where optimization values for Gaussian noise are reported for a single-relay system. We also notice that optimum values ξ and ψ_1 follow a certain pattern based on the SNR range of interest. For scenario 1, optimum value ξ remains almost constant for SNR range of 0 dB to 50 dB under consideration. For scenarios 2 and 3, ξ is nearly constant in low SNR region followed by a transition region in the region of 15-20 dB and then convergence to a constant value. We see similar trends for optimum values of ψ_1 .

In Table 4-2, we present optimization values ξ and ψ_1 for RB-CD scheme. φ_1 , φ_2 , A , and Γ are kept the same as in the STC-CD scheme. Modulation is chosen as 8-PSK. We observe from the table that ξ is almost constant for the whole range of SNR in scenario 1. However, in scenario 2 and 3, ξ values decrease in the region 0-10 dB, then increase in scenarios 2 and 3 in the range of 10-20 dB and 10-35 dB respectively. Then, ξ will in general decrease for both scenarios. A similar trend is observed for the values of ψ_1 for scenarios 1-3.

¹ Since optimization did not yield any significant performance improvement (as confirmed through simulations) in scenarios 4-6, optimum values for scenarios 4-6 were omitted from these tables.

Table 4-1: Optimum power allocation values for STC-CD in HI noise.

SNR [dB]	Scenario 1		Scenario 2		Scenario 3	
	ξ	ψ_1	ξ	ψ_1	ξ	ψ_1
0	0.9726	0.5000	0.7933	0.9919	0.9719	0.0001
5	0.9750	0.5000	0.7785	0.9946	0.7469	0.9957
10	0.9758	0.5000	0.7712	0.9954	0.7205	0.9970
15	0.9771	0.5000	0.7922	0.9943	0.7585	0.9957
20	0.9783	0.5000	0.9599	0.7276	0.9498	0.8308
25	0.9785	0.5000	0.9777	0.1161	0.9777	0.1179
30	0.9787	0.5000	0.9798	0.0071	0.9798	0.0001
35	0.9787	0.5000	0.9807	0.0001	0.9807	0.0001
40	0.9784	0.5000	0.9810	0.0001	0.9810	0.0001
45	0.9779	0.5000	0.8078	0.9941	0.9808	0.0001
50	0.9772	0.5000	0.7897	0.9950	0.9723	0.5060

Table 4-2: Optimum power allocation values for RB-CD in HI noise.

SNR [dB]	Scenario 1		Scenario 2		Scenario 3	
	ξ	ψ_1	ξ	ψ_1	ξ	ψ_1
0	0.9491	0.5000	0.7576	0.9018	0.7827	0.8830
5	0.9525	0.5000	0.7427	0.9165	0.7442	0.9130
10	0.9530	0.5000	0.7337	0.9217	0.7175	0.9255
15	0.9518	0.5000	0.7658	0.9026	0.7728	0.8978
20	0.9521	0.5000	0.8756	0.7852	0.9472	0.4527
25	0.9530	0.5000	0.8611	0.8159	0.9693	0.0631
30	0.9543	0.5000	0.8263	0.8649	0.9722	0.0053
35	0.9553	0.5000	0.8008	0.8903	0.9732	0.0005
40	0.9557	0.5000	0.7814	0.9041	0.9192	0.6901
45	0.9555	0.5000	0.7667	0.9119	0.8362	0.8601
50	0.9552	0.5000	0.7541	0.9172	0.7847	0.8990

4.2.2 Near Gaussian (NG) Noise

In Table 4-3 and 4-4, we present optimum values of ξ and ψ_1 for STC-CD and RB-CD schemes respectively, in NG noise. From these tables, we observe that for both schemes, values of ξ are almost constant through all considered values of SNR in scenario 1. In scenarios 2 and 3, ξ take values that are decreasing but approaching ~ 0.76 and ~ 0.68 respectively at high SNR for STC-CD scheme. As for the RB-CD scheme, values of ξ at high SNR are ~ 0.71 and ~ 0.66 for scenarios 2 and 3 respectively.

As for comparison of optimum values of ξ between HI and NG noise, we notice different trends. In HI noise for STC-CD scheme, values tend to increase followed by a constant region then decrease at high SNR. For RB-CD scheme, optimum values for scenarios 2 and 3 will have a slight initial decrease then a similar behavior as STC-CD scheme. However, in NG noise for both schemes, optimum values will tend to decrease throughout the range of SNR values.

Table 4-3: Optimum power allocation values for near Gaussian channel for STC-CD

SNR [dB]	Scenario 1		Scenario 2		Scenario 3	
	ξ	ψ_1	ξ	ψ_1	ξ	ψ_1
0	0.9741	0.5000	0.9771	0.0001	0.9771	0.0001
5	0.9764	0.5000	0.8118	0.9927	0.9795	0.0001
10	0.9767	0.5000	0.7912	0.9947	0.9800	0.0001
15	0.9765	0.5000	0.7787	0.9953	0.7499	0.9963
20	0.9762	0.5000	0.7707	0.9956	0.7213	0.9971
25	0.9760	0.5000	0.7655	0.9957	0.7051	0.9975
30	0.9758	0.5000	0.7620	0.9958	0.6953	0.9976
35	0.9756	0.5000	0.7589	0.9959	0.6869	0.9978
40	0.9755	0.5000	0.7574	0.9959	0.6833	0.9978
45	0.9754	0.5000	0.7564	0.9959	0.6808	0.9979
50	0.9754	0.5000	0.7555	0.9959	0.6788	0.9979

Table 4-4: Optimum power allocation values for near Gaussian channel for RB-CD

SNR [dB]	Scenario 1		Scenario 2		Scenario 3	
	ξ	ψ_1	ξ	ψ_1	ξ	ψ_1
0	0.9497	0.5000	0.7892	0.8835	0.9117	0.6764
5	0.9535	0.5000	0.7691	0.9058	0.8381	0.8505
10	0.9545	0.5000	0.7554	0.9152	0.7875	0.8955
15	0.9544	0.5000	0.7427	0.9206	0.7473	0.9162
20	0.9539	0.5000	0.7322	0.9238	0.7171	0.9272
25	0.9534	0.5000	0.7245	0.9257	0.6966	0.9330
30	0.9531	0.5000	0.7192	0.9269	0.6833	0.9363
35	0.9524	0.5000	0.7109	0.9285	0.6644	0.9402
40	0.9523	0.5000	0.7096	0.9287	0.6617	0.9407
45	0.9522	0.5000	0.7086	0.9289	0.6597	0.9411
50	0.9522	0.5000	0.7078	0.9290	0.6582	0.9414

Chapter 5

Simulation Results and Discussion

In this chapter, we present Monte Carlo simulation results to demonstrate the error rate performance of multi-relay system under impulsive noise assuming equal and optimum power allocation. We consider a two-relay cooperative system where the relays employ either Alamouti or repetition coding. To ensure a fair comparison in throughput rate, Alamouti and repetition-based schemes are simulated with 4-PSK and 8-PSK schemes, respectively.

5.1 BER Performance for OPA in Multi-Relay Channel

First, we analyze the effect of different degrees of impulsiveness on Alamouti-based scheme. In Figure 5.1, we present the simulated BER performance of the Alamouti-based scheme over Rayleigh fading channel in the presence of impulsive noise with various impulsiveness degrees. Specifically, we consider HI noise with $A = 10^{-4}$, moderate impulsive (MI) noise with $A = 10^{-2}$ and NG noise with $A = 1$. In all three noise environments, we have $\Gamma = 0.1$. The performance over Rayleigh fading channel in the presence of AWGN is also included as a benchmark. We consider scenario 1 where both relays are located close to destination.

As observed from Figure 5.1, the performance under impulsive noise dramatically differs from that of AWGN. The distinguishing characteristic of system behavior in HI noise is three-region performance; BER curve first decreases linearly with SNR, followed by a flat-region, finally decreasing again with increasing SNR. As the impulsive index gets larger, the flat-region tends to appear early, i.e., in the lower SNR region. Once the impulsive index is sufficiently large (i.e., channel tends to Gaussian), it disappears. It is also important to note that convergence to asymptotical diversity order is slower than we typically observe in a Rayleigh faded point-to-point multi-antenna diversity link with AWGN. This can be also verified due to the presence of Gamma function (as a result of cascaded channel structure over the relaying path) and summation term (as a result of impulsive noise) in the derived PEP expression given by (3.8).

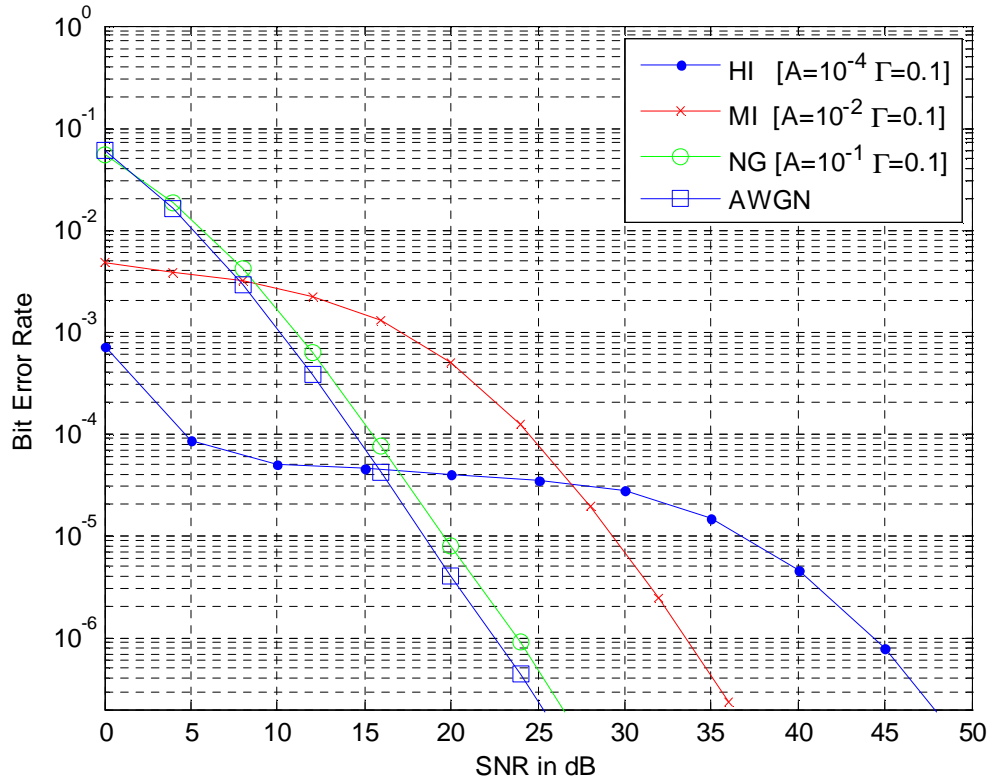


Figure 5.1: Performance of Alamouti-coded scheme in HI, MI and NG noise for scenario 1

In an attempt to demonstrate the effects of relays' location, we illustrate in Figure 5.2 the performance of the Alamouti-based scheme for scenarios 1-6. We assume HI noise with $A = 10^{-4}$ and $\Gamma = 0.1$. We observe from Figure 5.2 that the same diversity order is obtained irrespective of the location of relays. The best performance is however attained in scenario 4 where both relay nodes are located in the middle between source and destination nodes. The worst performance is observed in scenario 3 where one of the relays is closer to source node and the other relay is closer to destination node.

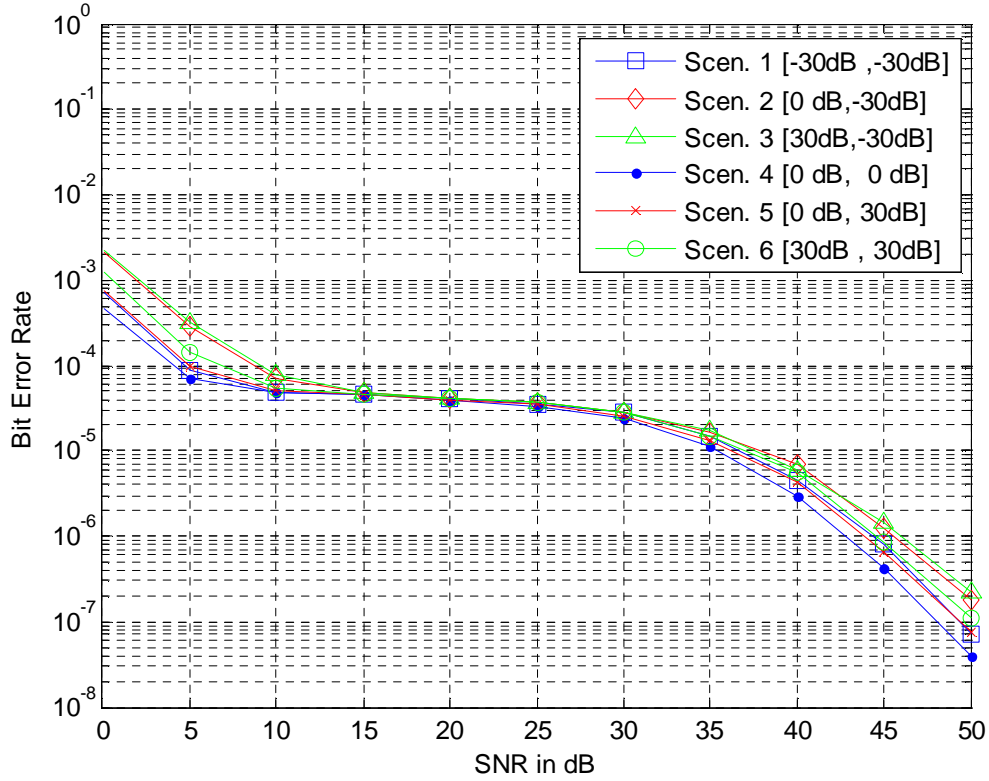


Figure 5.2: BER performance of Alamouti-coded scheme for various relays' locations

It is interesting to note that performance comparisons among these scenarios highly differ based on the coding employed across relay nodes. For instance, Figure 5.3 the performance of the repetition-based scheme for scenarios 1-6. We assume HI noise with $A = 10^{-4}$ and $\Gamma = 0.1$. As illustrated in Figure 5.3, repetition code based scheme yields the best performance in scenario 1 where both relays are located close to destination node. A further comparison between Figure 5.2 and Figure 5.3 reveal that, in scenarios 1-3, repetition-based cooperative scheme outperforms Alamouti-coded scheme by 1.5-3 dB at a target BER of 10^{-6} . On the other hand, scenarios 4-6 become favorable for Alamouti-coded scheme which outperforms repetition-based cooperative scheme by 1-2 dB at BER= 10^{-6} .

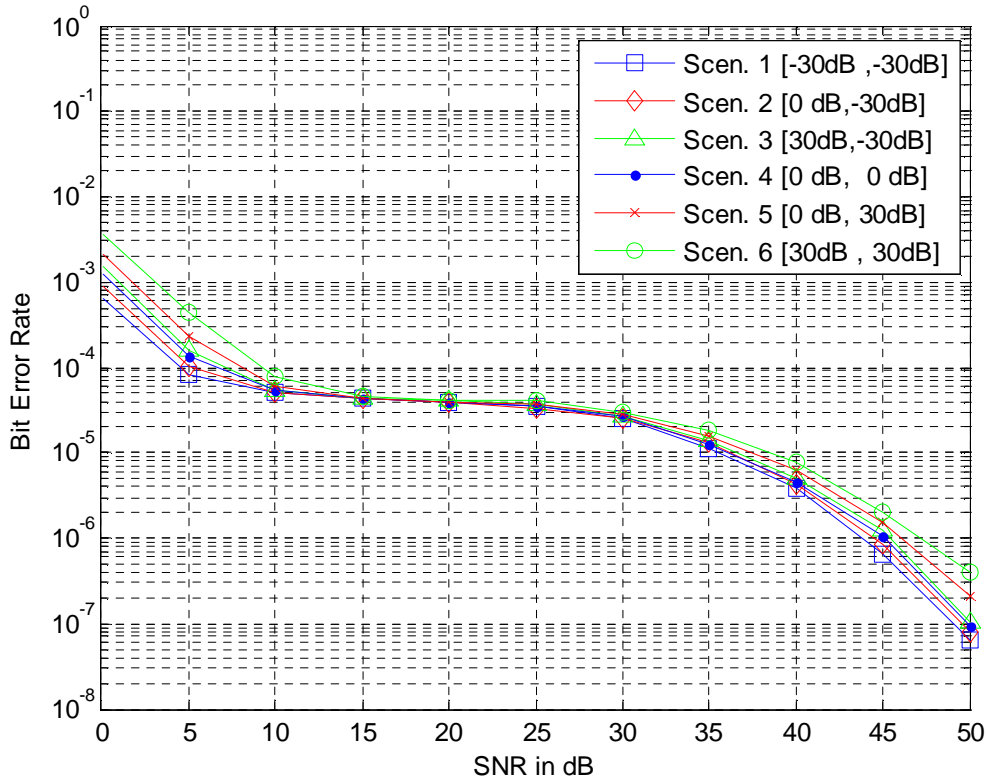


Figure 5.3: BER performance of repetition-based scheme for various relays' locations

To have further insight into the difference in BER performance between Alamouti-coded and repetition-based cooperative schemes, we investigate the derived PEP expressions in (3.8) and (3.15) respectively. Derived PEP expressions illustrated in Figure 5.4 and Figure 5.5 depict the difference in PEP values for scenarios 1-6 at SNR=22 dB. Best and worst scenarios for Alamouti-coded and repetition-based cooperative schemes can be readily noticed. For instance, worst performance in Alamouti-coded scheme is indicated by the maximum point in Figure 5.4, which corresponds to scenario 3. On the other hand, as observed from Figure 5.5, in repetition-based scheme the maximum value of PEP is encountered in scenario 6.

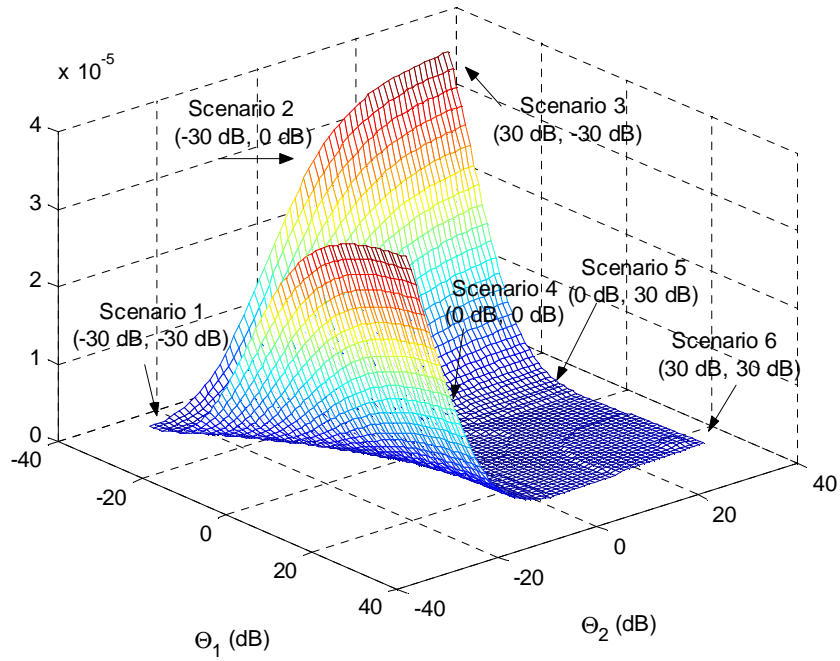


Figure 5.4: Derived PEP for Alamouti-coded cooperative scheme for different relays' locations

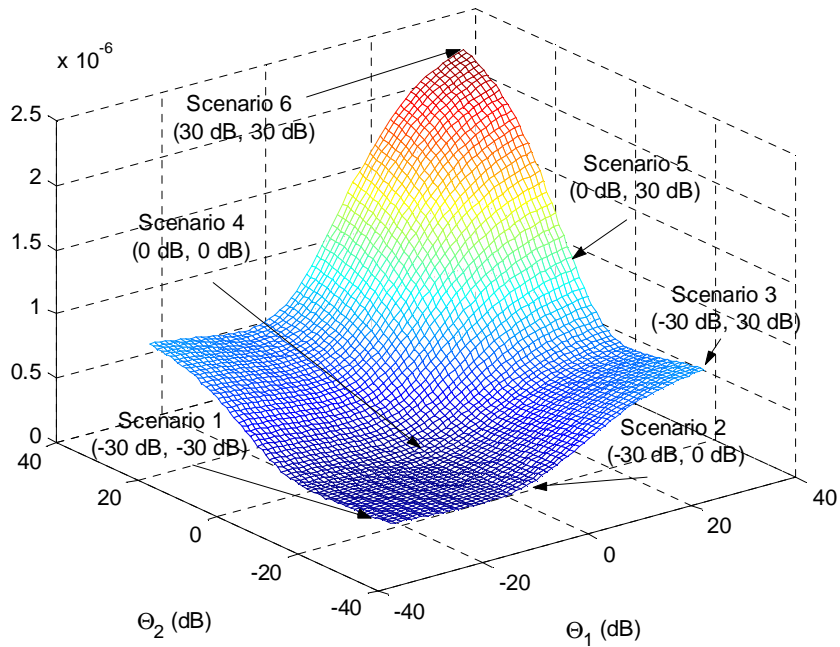


Figure 5.5: Derived PEP for repetition-based cooperative scheme for different relays' locations

In Figure 5.6 and Figure 5.7, we demonstrate the performance gains achieved through optimum power allocation (OPA) for Alamouti-based scheme in comparison to equal power allocation (EPA). In HI noise case illustrated in Figure 5.6, we observe gains in the range of 2-3 dB at $\text{BER}=10^{-6}$ depending on the relay locations. The gain is less as we move closer to the flat region. For example, at $\text{BER}=10^{-5}$, gains are in the range of 1-2 dB. In NG noise illustrated in Figure 5.7 we observe performance improvements of 2.5-5 dB at $\text{BER}=10^{-5}$. It turns out that OPA is more rewarding as the noise approaches to Gaussian nature.

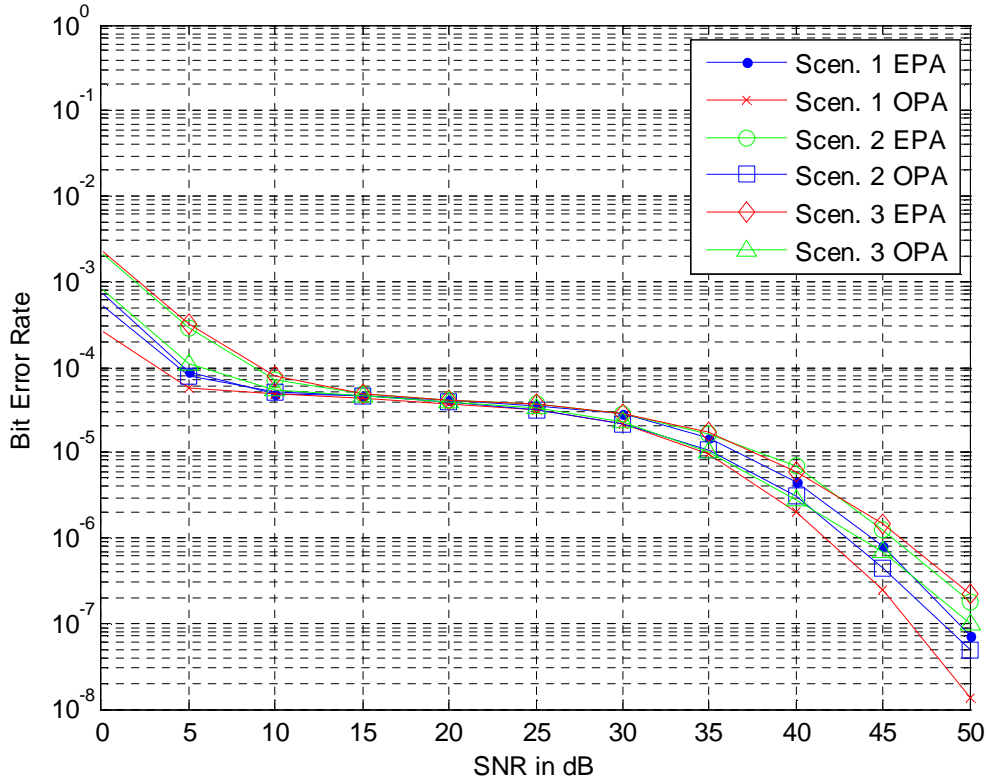


Figure 5.6: Performance comparison of OPA and EPA in HI noise for STC-CD scheme

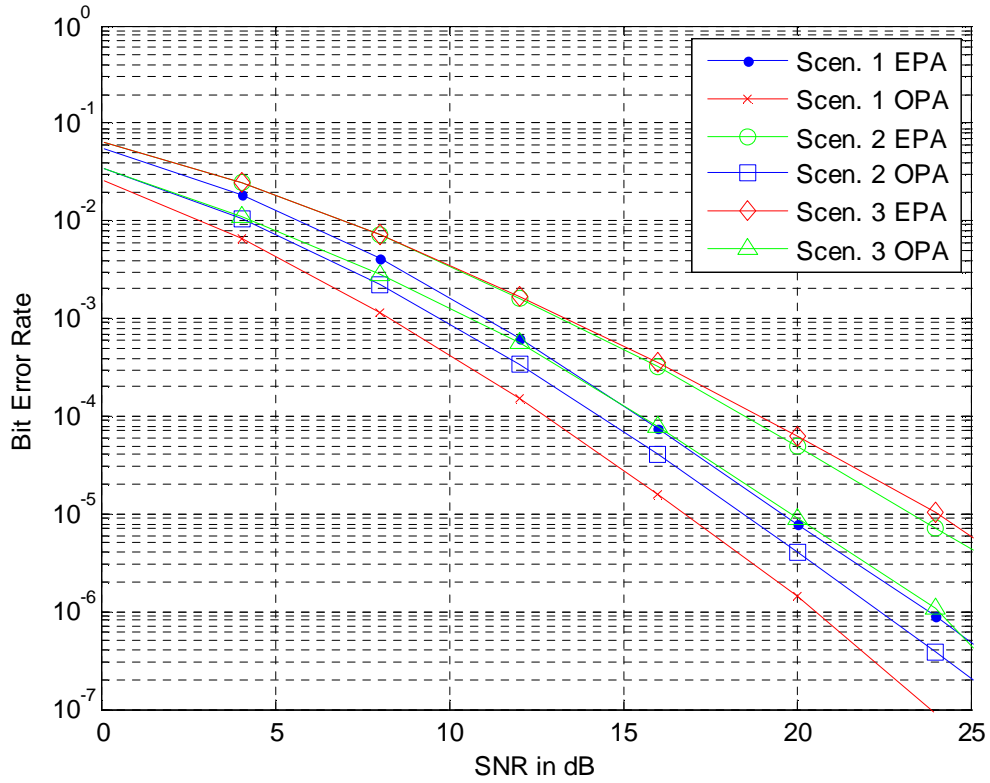


Figure 5.7: Performance comparison of OPA and EPA in near Gaussian channel

In Figure 5.8, we demonstrate the performance gains achieved through OPA for repetition-based scheme. We observe gains in the range of 2.5-3.5 dB at $\text{BER}=10^{-6}$ depending on the relays' locations. The gain is less as we move closer to the flat region. For example, at $\text{BER}=10^{-5}$, gains are in the range of 2-2.5 dB.

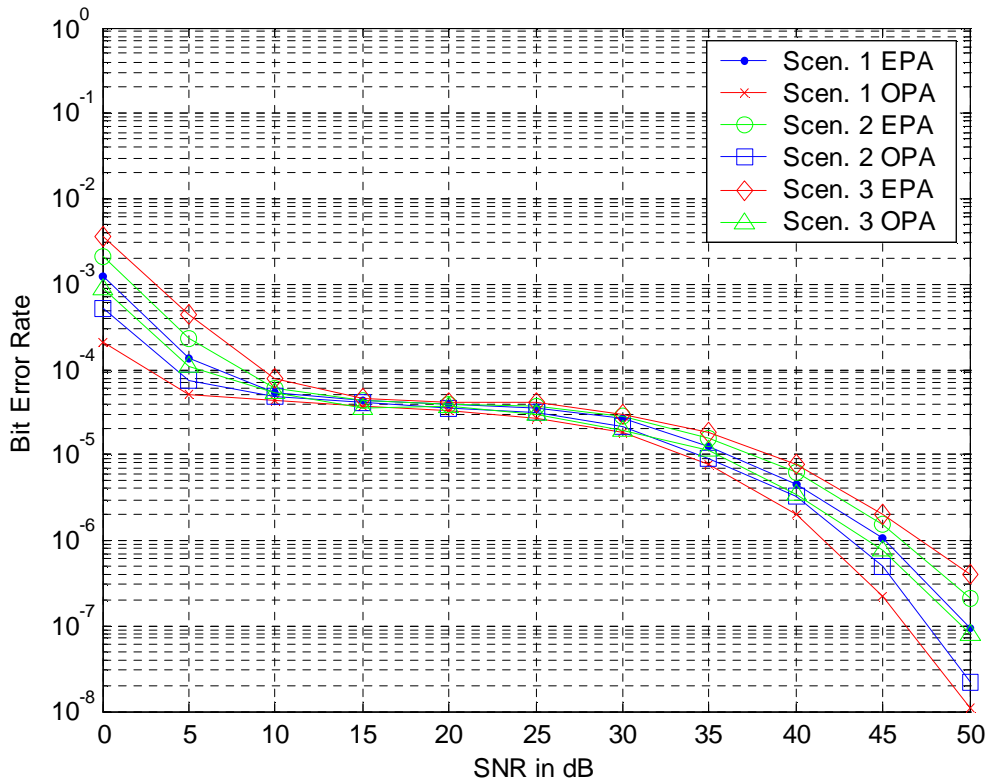


Figure 5.8: Performance comparison of OPA and EPA in HI noise for RB-CD scheme

So far we have assumed that noise samples are spatially dependent. In Figure 5.9, we demonstrate the effect of spatial independence on the BER performance. If the noise is highly impulsive and SNR values are sufficiently small (i.e., $\text{SNR} < 30$ dB), performance in spatially dependent noise is better than that in spatially independent case. In higher SNR region, this flips over and performance in spatially independent noise becomes better. On the other hand, both cases exhibit similar performance in NG noise, regardless of SNR region.

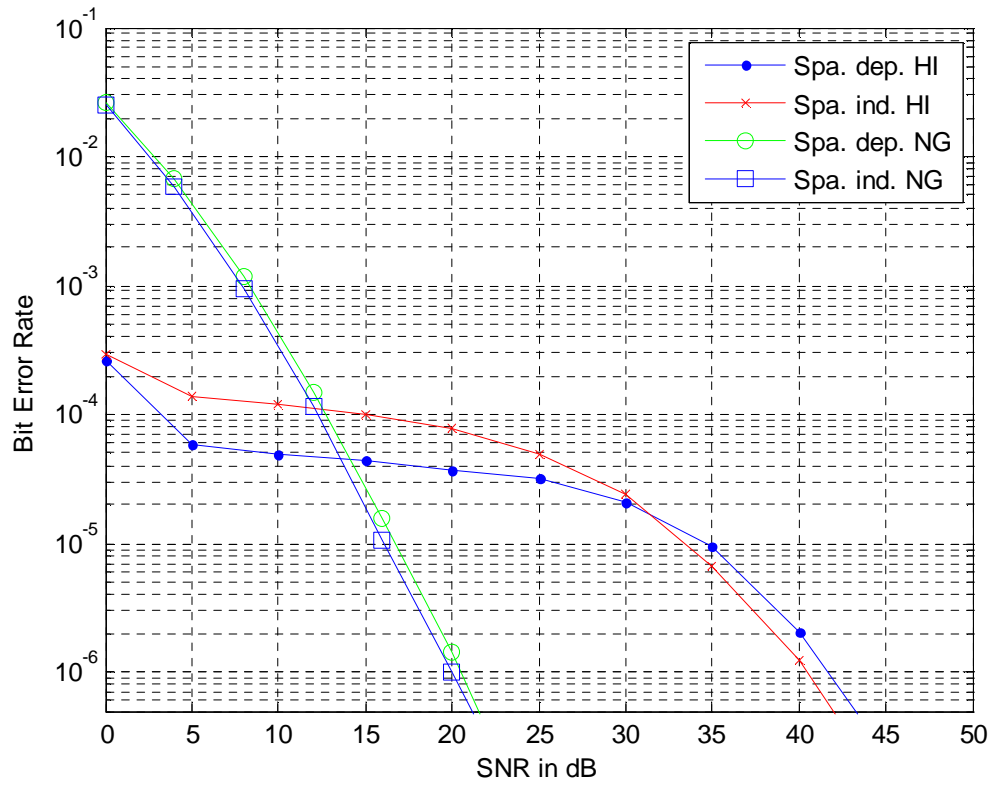


Figure 5.9: Performance comparison between spatially dependent and independent impulsive noise

Chapter 6

Conclusions

In this thesis, we have studied the performance of amplify-and-forward relaying schemes in the presence of impulsive noise. For a multi-relay scheme, we have derived PEP expressions assuming Rayleigh fading channel and Middleton Class A noise. We have considered both spatially dependent and independent interferers. The derived expressions include conventional AWGN as a special case and can be considered as a generalization of existing results in the literature. Through PEP, we have demonstrated that full spatial diversity can be extracted in highly impulsive noise environment for sufficiently high SNR values. The performance of cooperative system in lower SNR regions however depends on the impulsive nature of noise and different diversity orders dominate the performance in different ranges of SNRs. Based on a union bound on BER, we have further proposed power allocation rules for performance improvement. Performance gains up to 5 dB at $\text{BER}=10^{-5}$ have been observed depending on the relay geometry and impulsiveness degree.

Appendix

Appendix A - Convergence of (3.28) to $M + 1$

In this appendix, we demonstrate the convergence of the approximate diversity order for high SNR to the full spatial diversity order of the system, i.e. $M + 1$. Let $\gamma = E / N_0$, then

$$\lim_{\gamma \rightarrow \infty} d \cong \lim_{\gamma \rightarrow \infty} \left(-\gamma [A_1 + A_2 + A_3 + A_4] \right) \quad (\text{A.1})$$

Now, we have

$$\lim_{\gamma \rightarrow \infty} (-\gamma A_1) = \lim_{\gamma \rightarrow \infty} -\gamma \sum_{m=1}^M \left(\gamma^{-1} \exp \left(-\frac{4\Omega^2 \beta_1}{\eta_m \varepsilon_m^2} \gamma^{-1} \right) \left(\prod_{m=1}^M \Gamma_m \left(0, \frac{4\Omega^2 \beta_1}{\eta_m \varepsilon_m^2} \gamma^{-1} \right) \right)^{-1} \right) \quad (\text{A.2})$$

$$\lim_{\gamma \rightarrow \infty} \exp \left(-\frac{4\Omega^2 \beta_1}{\eta_m \varepsilon_m^2} \gamma^{-1} \right) = 1, \quad \forall m \in \{1, \dots, M\} \quad (\text{A.3})$$

$$\lim_{\gamma \rightarrow \infty} \Gamma_m \left(0, \frac{4\Omega^2 \beta_1}{\eta_m \varepsilon_m^2} \gamma^{-1} \right) = \lim_{\gamma \rightarrow \infty} \int_{\frac{4\Omega^2 \beta_1}{\eta_m \varepsilon_m^2} \gamma^{-1}}^{\infty} t^{-1} e^{-t} dt = \int_0^{\infty} t^{-1} e^{-t} dt = \Gamma(0) = \infty, \quad \forall m \in \{1, \dots, M\} \quad (\text{A.4})$$

After further manipulation of (A.2) and using (A.3) and (A.4), we obtain

$$\lim_{\gamma \rightarrow \infty} (-\gamma A_1) = 0 \quad (\text{A.5})$$

In addition, we have

$$\lim_{\gamma \rightarrow \infty} (-\gamma A_2) = \lim_{\gamma \rightarrow \infty} \beta_1 \gamma^{-1} \left(\sum_{m=1}^M \left(\frac{\eta_m \varepsilon_m^2}{4\Omega^2} \right)^{-1} \right) = 0 \quad (\text{A.6})$$

$$\lim_{\gamma \rightarrow \infty} (-\gamma A_3) = M \quad (\text{A.7})$$

$$\lim_{\gamma \rightarrow \infty} (-\gamma A_4) = 1 \quad (\text{Using l'Hôpital's rule}) \quad (\text{A.8})$$

Therefore, from (A.5)-(A.8), we conclude

$$\lim_{\gamma \rightarrow \infty} d = M + 1 \quad (\text{A.9})$$

Bibliography

- [1] A. Goldsmith, *Wireless Communication*, Cambridge University Press, 2005.
- [2] V. Tarokh, N. Seshadri, and A. R. Calderbank, "Space-time codes for high data rate wireless communication: Performance criterion and code construction," *IEEE Trans. Inf. Theory*, vol. 44, no. 2, pp. 744-765, Mar. 1998.
- [3] A. Nosratinia, T. E. Hunter, and A. Hedayat, "Cooperative communication in wireless networks," *IEEE Commun. Mag.*, vol. 42, no. 10, pp. 74-80, Oct. 2004.
- [4] F. H. P. Fitzek and M. D. Katz (Eds.), *Cooperation in Wireless Networks: Principles and Application Real Egoistic Behavior is to Cooperate!*, 1st edition, Dordrecht, Netherlands: Springer, 2006.
- [5] M. Uysal (Ed.), *Cooperative Communications for Improved Wireless Network Transmission: Frameworks for Virtual Antenna Array Applications*, 1st edition, IGI Global, 2009.
- [6] D. Middleton, "Man-made noise in urban environments and transportation systems: Models and measurements," *IEEE Trans. Commun.*, vol. 21, no. 11, pp. 1232-1241, Nov. 1973.
- [7] E. N. Skomal, "The range and frequency dependence of VHF-UHF man-made radio noise in and above metropolitan areas," *IEEE Trans. on Veh. Technol.*, vol. 19, no. 2, pp. 213-221, May 1970.
- [8] K. L. Blackard, T. S. Rappaport, and C. W. Bostian, "Measurements and models of radio frequency impulsive noise for indoor wireless communications," *IEEE J. Select. Areas in Commun.*, vol. 11, no. 7, pp. 991-1001, Sept. 1993.
- [9] M. S. Kuran and T. Tugcu, "A survey on emerging broadband wireless access technologies," *Computer Networks*, vol. 51, no. 11, pp. 3013-3046, Jan. 2007.
- [10] T. K. Blankenship and T. S. Rappaport, "Characteristics of impulsive noise in the 450-MHz band in hospitals and clinics," *IEEE Trans. Antennas Propag.*, vol. 46, no. 2, pp. 194-203, Feb. 1998.
- [11] M. G. Sanchez, A. V. Alejos, and I. Cuinas, "Urban wide-band measurement of the UMTS electromagnetic environment," *IEEE Trans. Veh. Technol.*, vol. 53, no. 4, pp. 1014-1022, Jul. 2004.
- [12] H. M. Hall, "A new model for impulsive phenomena: Application to atmospheric-noise communication channels," *Stanford Univ., Tech. Rep.*, Aug. 1966.
- [13] E. Conte, M. Di Bisceglie, and M. Lops, "Optimum detection of fading signals in impulsive noise," *IEEE Trans. Commun.*, vol. 43, no. 4, pp. 869-876, Apr. 1995.

- [14] S. Buzzi, E. Conte, and M. Lops, "Optimum detection over Rayleigh-fading, dispersive channels, with non-Gaussian noise," *IEEE Trans. Commun.*, vol. 45, no. 9, pp. 1061-1069, Sept. 1997.
- [15] M. Shao and C. L. Nikias, "On symmetric stable models for impulsive noise," *Univ. Southern California, Los Angeles, Tech. Rep. USC-SIPI-231*, 1993.
- [16] D. Middleton, "Statistical-physical models of electromagnetic interference," *IEEE Trans. Electromagn. Compat.*, vol. EMC-19, no. 3, pp. 106-127, Aug. 1977.
- [17] D. Middleton, "Canonical and quasi-canonical probability models of class A interference," *IEEE Trans. Electromagn. Compat.*, vol. EMC-25, no. 2, pp. 76-106, May 1983.
- [18] J. W. Mark and W. Zhuang, *Wireless Communications and Networking*, 1st edition, Prentice Hall, 2002.
- [19] J. G. Proakis, *Digital Communications*, 4th edition, McGraw-Hill, 2001.
- [20] D. Tse and P. Viswanath, *Fundamentals of Wireless Communication*. Cambridge University Press, 2005.
- [21] A. Wittneben, "Base station modulation diversity for digital simulcast," *IEEE Veh. Technol. Conf., 'Gateway to the Future Technology in Motion'*, pp. 848-853, May 1991.
- [22] V. Kuhn, *Wireless Communications Over MIMO Channels: Applications to Cdma and Multiple Antenna Systems*, 1st edition, John Wiley & Sons, 2006.
- [23] S. M. Alamouti, "A simple transmit diversity technique for wireless communications," *IEEE J. Sel. Areas Commun.*, vol. 16, no. 8, pp. 1451-1458, Oct. 1998.
- [24] V. Tarokh, H. Jafarkhani, and A. R. Calderbank, "Space-time block codes from orthogonal designs," *IEEE Trans. Inf. Theory*, vol. 45, no. 5, pp. 1456-1467, Jul. 1999.
- [25] J. Radon, "Lineare Scharen orthogonaler Matrizen," *Abh. Math. Sem. Univ. Hamburg*, vol. 1, pp. 1-14, 1922.
- [26] E. Biglieri, G. Taricco, and A. Tulino "Performance of space-time codes for a large number of antennas," *IEEE Trans. Inf. Theory*, vol. 48, no. 7, pp. 1794-1803, Jul. 2002.
- [27] Z. Chen, J. Yuan, and B. Vucetic, "An improved space-time trellis coded modulation scheme on slow rayleigh fading channels," *Communications, ICC 2001. IEEE International Conference*, 2001,
- [28] D. M. Ionescu, "On space-time code design," *IEEE Trans. Wireless Commun.*, vol. 2, no. 1, pp. 20-28, Jan. 2003.

- [29] M. Tao and R. S. Cheng, "Improved design criteria and new trellis codes for space-time coded modulation in slow flat fading channels," *IEEE Commun. Lett.*, vol. 5, no. 7, pp. 313-315, Jul. 2001.
- [30] G. J. Foschini, "Layered space-time architecture for wireless communication in a fading environment when using multiple antennas," *Bell Labs Technical Journal*, vol. 1, pp. 41-59, 1996.
- [31] H. E. Gamal and A. R. Hammons Jr., "A new approach to layered space-time coding and signal processing," *IEEE Trans. Inf. Theory*, vol. 47, no. 6, pp. 2321-2334, Sept. 2001.
- [32] B. Hassibi and B. M. Hochwald, "High-rate codes that are linear in space and time," *IEEE Trans. Inf. Theory*, vol. 48, no. 7, pp. 1804-1824, Jul. 2002.
- [33] R. W. Heath Jr. and A. J. Paulraj, "Linear dispersion codes for MIMO systems based on frame theory," *IEEE Trans. Signal Process.*, vol. 50, no. 10, pp. 2429-2441, Oct. 2002.
- [34] J. N. Laneman and G. W. Wornell, "Distributed space-time-coded protocols for exploiting cooperative diversity in wireless networks," *IEEE Trans. Inf. Theory*, vol. 49, no. 10, pp. 2415-2425, Oct. 2003.
- [35] J. N. Laneman, D. N. C. Tse, and G. W. Wornell, "Cooperative diversity in wireless networks: Efficient protocols and outage behavior," *IEEE Trans. Inf. Theory*, vol. 50, no. 12, pp. 3062-3080, Dec. 2004.
- [36] R. U. Nabar, H. Bolcskei, and F. W. Kneubuhler, "Fading relay channels: Performance limits and space-time signal design," *IEEE J. Select. Areas Commun.*, vol. 22, no. 6, pp. 1099-1109, Aug. 2004.
- [37] A. Sendonaris, E. Erkip, and B. Aazhang, "User cooperation diversity-part I: System description," *IEEE Trans. Commun.*, vol. 51, no. 11, pp. 1927-1938, Nov. 2003.
- [38] A. Sendonaris, E. Erkip, and B. Aazhang, "User cooperation diversity-part II: Implementation aspects and performance analysis," *IEEE Trans. Commun.*, vol. 51, no. 11, pp. 1939-1948, Nov. 2003.
- [39] E. C. Van der Meulen, "Three-terminal communication channels," *Adv. Appl. Prob.*, vol. 3, no. 1, pp. 120-154, 1971.
- [40] A. Sendonaris, E. Erkip, and B. Aazhang, "Increasing uplink capacity via user cooperation diversity," in *Proc. IEEE International Symposium on Inf. Theory*, Aug. 1998.
- [41] J. N. Laneman and G. W. Wornell, "Energy-efficient antenna sharing and relaying for wireless networks," *IEEE Wireless Commun. and Networking Conf.*, 2000.

- [42] A. Spaulding and D. Middleton, "Optimum reception in an impulsive interference environment-part I: Coherent detection," *IEEE Trans. Commun.*, vol. 25, no. 9, pp. 910-923, Sept. 1977.
- [43] A. Spaulding and D. Middleton, "Optimum reception in an impulsive interference environment-part II: Incoherent reception," *IEEE Trans. Commun.*, vol. 25, no. 9, pp. 924-934, 1977.
- [44] R. Haring and A. J. Han Vinck, "Performance bounds for optimum and suboptimum reception under class-A impulsive noise," *IEEE Trans. Commun.*, vol. 50, no. 7, pp. 1130-1136, Jul. 2002.
- [45] C. Tepedelenlioglu and P. Gao, "On diversity reception over fading channels with impulsive noise," *IEEE Trans. Veh. Technol.*, vol. 54, no. 6, pp. 2037-2047, Nov. 2005.
- [46] P. Gao and C. Tepedelenlioglu, "Space-time coding over fading channels with impulsive noise," *IEEE Trans. Wireless Commun.*, vol. 6, no.1, pp. 220-229, Jan. 2007.
- [47] M. M. Fareed and M. Uysal, "BER-optimized power allocation for fading relay channels," *IEEE Trans. Wireless Commun.*, vol. 7, no. 6, pp. 2350-2359, Jan. 2008.
- [48] P. A. Delaney, "Signal detection in multivariate class-A interference," *IEEE Trans. Commun.*, vol. 43, no. 2, pp. 365-373, Feb. 1995.
- [49] I. S. Gradshteyn and I. M. Ryzhik, *Table of Integrals, Series, and Products*, Academic Press, 5th edition, 1994.
- [50] R. Narasimhan, "Finite-SNR diversity-multiplexing tradeoff for correlated Rayleigh and Rician MIMO channels," *IEEE Trans. Inf. Theory*, vol. 52, no. 9, pp. 3965-3979, Sept. 2006.
- [51] S. Benedetto and E. Biglieri, *Principles of Digital Transmission with Wireless Applications*, Norwell, USA: Kluwer Academic Publishers, 1999.
- [52] The MathWorks, *Optimization Toolbox 4 User's Guide*, The Mathworks Inc., 2008.